CHAPTER ONE
INTRODUCTION

1.1 Introduction:

The determination of the pavement thicknesses was based purely on experiments until the 1920 years. These experiments were developed also with the time. The rigid pavements, like those of conventional concretes, can be analyzed by the plate theory. The plate theory supposes that the concrete slab is a medium thickness plate with plane sections before and after strains. If the wheel is placed close to the center of the slab, then only the plate's theory can be used for the rigid pavements. The plate's theory or the layer's theory can be used when the load is applied to the slab center (Zdiri, 2009).

The design methods were developed by various organizations for the determination of the necessary thicknesses of pavements. The analytical solutions, developed thereafter, vary from the "Closed-form Formulas" to the complex derivations which are valid for the determination of the stress and the deflection in the rigid pavements. But with the development of the powerful finite element method, is notice a significant evolution in the analysis of the rigid pavements. Various finite element models have been developed for analyzing the behavior of concrete pavement systems. For these analyses, computer programs were developed by using the finite element method such as ILLI-SLAB, WESLIQID, J-SLAB, FEACONS-IV, SLAB2000, WESLAYER , ABAQUS and ANSYS .The main advantage of these approaches is the evaluation of the critical load transfer phenomena and the stress distributions in the rigid pavements like the roller compacted concrete (RCC) slabs. Many researchers employed the finite element packages in order to analyze the behavior of concrete pavements. This enabled the prediction of stresses and displacements (Modelling of the Stresses and Strains Distribution in an RCC Pavement Using the Computer Code "Abaqus" (Zdiri, 2009).

In 2011 the Federal Aviation Administration (F.A.A) developed 3D Finite Element program (FEAFAA 1.2) uses for analysis airport rigid pavement (Brill, 2011).

Using ANSYS software a model can be developed for the study of airport rigid pavements and its foundation. For such a study 3D finite element models are developed using FE program to obtain results which are compared with analytical models results.

1.2 Problem Statement

The structural analysis of highway and airports rigid pavements has mostly centered on the evaluation of stress. The overstress giving rise to cracking in the structure has been considered as a principal indicator of failure of pavements. In turn, design of airport concrete pavements has centered on avoiding the formation of such cracking by keeping the level of stress below the allowable concrete strength . The use of the finite element method enables the accurate prediction of stresses and displacement. Thus the development of 3D finite element model for the analysis and design of rigid runway pavements is required.

1.3 Objectives

The main objective of this study is to develop and implement a pavement response model using a finite element program in predicting stresses and deflections in rigid pavements.

The specific objectives are:

1. To study the importance of the improvement of stress prediction to provide safe design.
2. To learn how to use the finite element method in the analysis of rigid pavements.
3. To develop 3D finite element model for the analysis and design of rigid runway pavements using ANSYS program.
4. To predict the displacement and stress that cause premature failure
5. To verify the accuracy of the result of the model by comparison with published results.

1.4 Methodology

The following steps are performed:

1. Collect data of materials prosperities and design thickness of rigid pavement from F.A.A international report.
2 Analyze data and calculate the stress and deflection using Westergaard theory.
3 Use Finite element program (ANSYS) to create a rigid pavement model and apply the load with the given materials properties.

5. Compare the results of model with the result of analytical method and draw calculations and present recommendations.

1.5 Outlines of Thesis

Chapter one provides information about the nature of this study and discusses the research problem. It contains the introduction, problem, objectives, and methodology.

Chapter Two oriented as a literature review about "Modelling of stress and deflection of airport rigid pavement using finite element analysis". It focuses on the part "rigid pavement response model". It also illustrates the general methods and previous studies used in analysis of concrete pavement.

Chapter Three emphasizes on "Methods of analysis and design". It illustrates in detail the equations and theories used in analysis and design of concrete pavement.

Chapter Four discusses the results of analysis method including analytical method and finite element analysis.

Finally, chapter Five summarizes the findings and conclusions of this research as well as the suggested recommendations.

CHAPTER TWO
LITERTURE REVIEW

2.1 Background:

Pavement structural analysis includes three main issues material characterization theoretical model for structural response and environmental conditions .Three aspects of the material behavior are typically considered for pavement analysis (Yoder and Witczak, 1975):

(1) The relationship between the stress and strain (linear or nonlinear).

(2) The time dependency of strain under a constant load (viscous or non viscous);

(3) The degree to which the material can recover strain after stress removal (elastic or plastic).

Theoretical response models for the pavement are typically based on a continuum mechanics approach. The model can be a closed-formed analytical solution or a numerical approach. Various theoretical response models have been developed with different levels of sophistication from analytical solutions such as Boussinesq's equations based on elasticity to three-dimensional dynamic finite element models (Wei Tu, 2007).

2.2 Rigid Pavement Response Models

Because of concrete's high elastic modulus, the Portland cement concrete (PCC) slab supplies most of the structural capacity, and tends to transfer the traffic loads to a relatively wider area than does asphalt, producing a very different stress distribution from the one generated by a flexible pavement. Furthermore, variable slab sizes, the presence of different types of discontinuities (longitudinal and transverse joints), a variety of load transfer mechanisms (dowel bars and aggregate interlocks), and high sensitivity to environmental conditions (temperature curling and moisture warping) make the analysis of rigid pavement a more complicated and challenging problem. The multi-layer elastic theory is generally not considered an appropriate tool for rigid pavement response analysis (Wei Tu, 2007).

2.2.1 Westergaard's Analytical Solution

The early advances in rigid pavement analysis started in the 1920s. In 1926, Westergaard derived closed form analytical solutions for stresses and deflections due to thermal curling and traffic loading in jointed rigid pavements. To simplify the problem, he assumed that the subgrade cannot transfer shear

stresses. The subgrade is characterized by a single parameter, the modulus of subgrade reaction or the k value. The vertical pressure of the subgrade to the concrete slab is a constant which equals to subgrade reaction (k) times the vertical deflection. The following assumptions were made in Westergaard's original work (Westergaard, 1926a):

1) The concrete slab acts as a homogeneous, isotropic, elastic solid in equilibrium;

2) The classic Kirchhoff plate theory is assumed for the concrete slab and the transverse shear stresses are ignored;

3) The reaction of the subgrade is only vertical and is proportional to the deflection of the slab.

4) The concrete is resting on a set of springs with the spring constant k , independent of the slab deflection.

5) The thickness of the slab is uniform

6) Three loading conditions are considered: interior, corner, and edge.

7) The loading pressure is assumed to be distributed uniformly over a circular or semi-circular area with radius (a) shows in (Figure 2.1)

8) The slab is only subjected to one load.

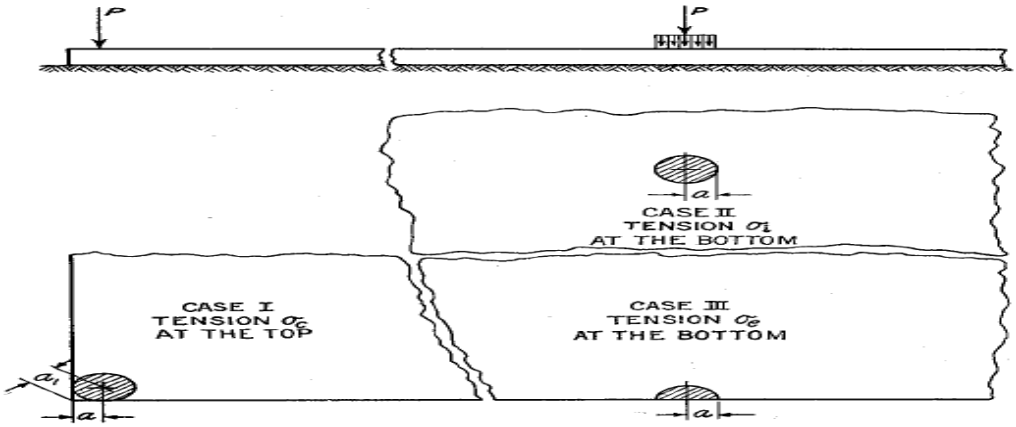

Figure 2.1 Three Loading Conditions for Westergaard Equations (Westergaard, 1926a)

2.2.2 Improved Models Based on Westergaard's Theory

Since Westergaard's original work, some researchers have made improvements on Westergaard's theory. Pickett and Ray (1951) developed influence charts that allow the Westergaard equations to be applied to multiple wheel loadings. Two cases were considered in their study: the Winkler (dense liquid) subgrade and the elastic solid subgrade. Pickett and Ray's influence charts have been

used by the Portland Cement Association (PCA) for rigid pavement design. The charts for interior loading were used for the design of airport pavements (PCA, 1955).

As stated by Wie Tu, 2007, "Salsilli et al. (1993) applied the Newton-Raphson iteration procedure to convert multiple wheel loadings to an equivalent single loaded area that would produce the same bending stress and used this transformed loading in Westergaard's equations. Three-wheel load configurations were considered: dual, tandem and tridem"

2.2.3 Finite Element Models

Although closed-form analytical solutions are very desirable for practicing engineers in routine pavement analysis and design, the assumptions made to develop those solutions place too many limitations on the application. To overcome the limitations of analytical solutions, the finite element method has become a widely used tool for rigid pavement analysis since the early 1970s.

Chen etal (2002) presented a review including the following studies of the pavement finite element modelling:

1. Wang and his colleagues (1972) study of the responses of rigid pavements to wheel loads using a two dimensional (2D) linear elastic finite element model. The concrete slab was modeled with medium-thick plate elements assuming the classical plate theory based on Kirchhoff hypothesis.. Stresses and deflections computed with the finite element model were compared with those from Westergaard's equations. The comparison showed that the analytical solutions give lower stresses and deflections.

2. Huang (1974) study presenting another 2D elastic finite element model for rigid pavements. In his model, the foundation was modeled as an elastic continuum and the effect of load transfer from adjacent slabs and loss of contact were considered as well.

3. Following the early developments of 2-D elastic finite element models, Tabatabaie and Barenberg (1978, 1980) development of a more general 2-D finite element program called ILLI-SLAB. The concrete slab was modeled using medium-thick elements like earlier models but the effect of bonded or unbonded base layer could be incorporated using a second layer of plate elements below the slab. The subgrade was modeled as Winkler foundation and dowel bars at joints were modeled as discrete bar elements.

4. The modification and extension by Chou (1981) The 2-D finite element program developed by Huang and Wang (1973). Two programs were developed: WESLIQID and WESLAYER. Both programs were based on the classical medium-thick plate theory. The main difference between the two was the subgrade modeling.

5. Huang (1983), Huang and Deng (1985) extension of the earlier model KENSLABS to include the capability of modeling multiple slabs and various load transfer mechanisms in a manner similar to the ILLI-SLAB. The subgrade was characterized as an elastic half space. The loss of subgrade contact and the effects of mesh refinement were also studied.

6. The development of a finite element program called RISC as part of a mechanistic design procedure for rigid pavements for FHWA (Majidzadeh et al. 1984). In this program, the concrete slab was modeled using thin elastic shell element assuming Kirchhoff's theory.

7. Tayabji and Colley (1984) development of a 2D finite element program called JSLAB to analyze jointed reinforced concrete pavements. The slab was modeled using medium thick plate elements. The subgrade was modeled as a Winkler foundation.

8. Tia et al. (1987) development of a 2D finite element program named FEACONS (Finite Element Analysis of Concrete Slabs) to analyze the response of jointed concrete pavements to load and temperature variations. Similar to other 2-D finite element program, the concrete slab was modeled using medium-thick plate elements while the subgrade was assumed as a Winkler foundation.

9. Krauthammer and Western (1988) investigation of the effects of shear transfer on pavement behavior using a 2D plane strain dynamic finite element model developed in the commercially available finite element program ADINA..

10. Ioannides and Donnelly (1988) examination of the effect of subgrade nonlinearity using a existing 3D finite element program called GEOSYS. Linear 8-node brick elements were used to model the slab and subgrade, with varying degree of mesh refinement.
11. Channakeshava et al. (1993) development of a 3-D, nonlinear static finite element model to study the 3-D response of plain concrete with doweled joints. The slab were modeled with 20-node, quadratic isoparametric brick elements. The subgrade was modeled as a Winkler foundation with

three discrete linear springs at each node on the base of the slab. Both wheel loads and thermal loading induced by diurnal temperature cycling were considered in their study.

12. Zaghloul et al. (1994) investigation of the load equivalent factors by using a 3-D, nonlinear dynamic finite element model with the commercially available finite element program ABAQUS. The slab and subgrade were modeled with 3-D brick elements. The concrete was modeled as a bilinearly elastic-plastic solid. The granular base, subbase and subgrade were modeled with an elastic-plastic Druker-Prager model. The clayey subgrade was modeled using a Cam-Clay model. The predicted deflections for the static loading condition were compared with those determined from Westergaard's analytical solution and a separate finite element program to verify the model..

13. Chatti et al. (1994) extension of the existing static 2-D model ILLI-SLAB to a linear dynamic finite element program, called DYNA-SLAB, to study the effects of dynamic loading applied by trucks on the response of rigid pavements. The concrete slab was modeled with plate elements and the foundation was treated as a Winkler foundation or a layered visco-elastic medium over a rigid or an infinite half-space.

14. Uddin et al. (1995) report on a study of the effect of pavement discontinuities on surface deflections of a rigid pavement subjected to a standard FWD load using a 3-D elastic finite model with the general purpose finite element program ABAQUS. The concrete slab, cement-treated base, and subgrade were modeled using 3-D elastic brick elements. Cracks in the pavement were modeled using gap elements while dowels were modeled with beam elements.

15. Kuo et al. (1995) development of a 3D elastic finite element model using ABAQUS to investigate the various factors affecting rigid pavement support including base thickness and stiffness, interface bonding, slab curling and warping due to temperature and moisture gradient, load transfer at the joints and lane widths. Significant effort was made to determine the optimum mesh refinement and best element type. The subgrade was treated as a Winkler foundation. The interface between layers was modeled using a membrane element coupled with a special interface element. The model was verified by comparing the model predictions with both Westergaard's analytical solution and the predictions from the 2D finite element model ILLI-SLAB.

16. Zaman and Alvappillai (1995) study of the effect of moving aircraft loads on a jointed multi-slab rigid pavement system using a 2-D dynamic finite element model. The pavement slabs were modeled using 4-noded, rectangular medium-thick plate elements. The subgrade was treated as a viscoelastic Winkler foundation. The dynamic interaction between the aircraft and pavement was modeled using a parallel spring and dashpot with an associated mass. Longitudinal joints were modeled using discrete displacement springs while transverse joints were modeled as doweled, and debonding and gaps between dowels and slabs were allowed.

17. Masad et al. (1996) development of a 3-D finite element model using ABAQUS to examine the response of rigid pavements to the thermal loading. Both the slab and subgrade were modeled with 8-noded brick elements. The slab and foundation were both assumed to be linearly elastic. Longitudinal joints, friction and loss of contact between the slab and foundation were considered in the analysis. Both linear and nonlinear temperature gradients were examined.

18. Study reported by Kim et al. (1997), a 3D elastic finite element model was developed using ABAQUS to analyze the response of a single rigid pavement slab to the heavy multiple-wheel loading applied by aircraft landing. The slab, cement-treated base, and subgrade were modeled using linear hexahedral elements. Bonded and unbonded bases were considered in the analyses.. Different wheel configurations were examined including single, dual, and triple tandem axle loading.

19. Brill et al. (1997) development of a 3D static finite element model for rigid pavements using the public domain finite element program NIKE3D. Unlike most 3D finite element models, the slab was modeled with 4 noded plate elements while the subgrade was modeled using linear 8 noded hexahedral elements. Different types of joints between slabs were considered, including aggregate interlock and dowel shear transfer mechanism modeled with linearly elastic hexahedral elements.

20. 3D static finite element model, EVERFE, was development of by Davids (1998) to model the response of jointed plain concrete pavement systems to wheel loads and environmental effects. The slab, base, and subgrade were modeled using 20 noded quadratic hexahedral elements. All pavement layers were treated as linearly elastic materials. A Winkler foundation was modeled below the subgrade using an 8-noded quadratic interface element. The dowel and aggregate interlock mechanisms were modeled with specialized elements and constitutive relations. Linear,

bilinear, and trilinear thermal gradients through the slab thickness were simulated.

As stated by Wie, 2007, all the finite element models that have been developed for rigid pavement analysis are based on displacement formulations. In a displacement based finite element model, the displacement functions are assumed. The displacements at the nodes of the elements are calculated first as the primary variables. Then the stresses and strains, which are more important for design purposes, are calculated by numerically differentiating the approximate solutions. In a pavement structure, the interfaces between layers are usually locations of large stress and strain gradients because of the discontinuity in material properties. Although accurate displacement and in-plane stress distributions can be predicted, predictions of transverse stress distributions across the pavement thickness are generally not accurate due to the inherent limitations of displacement based approaches.

CHAPTER THREE
METHODS OF ANALYSIS AND DESIGN

3.1Introduction:

Three methods can be used to determine the stresses and deflections in concrete pavements: closed-form formulas, influence charts, and finite element computer programs. The formulas originally developed by Westergaard can be applied only to a single wheel load with a circular, semicircular, elliptical, or semielliptical contact area. The influence charts developed by Pickett and Ray (1951) can be applied to multiple wheel loads of any configuration. Both methods are applicable only to a large slab on a liquid foundation. If the loads are applied to multiple slabs on a liquid, solid, or layer foundation with load transfer across the joints, the finite-element method should be used. The liquid foundation assumes the subgrade to be a set of independent springs. Deflection at any given point is proportional to the force at that point and independent of the forces at all other points. This assumption is unrealistic and does not represent soil behaviors. Due to its simplicity, it was used in Westergaard's analysis. However, with the ever-increasing speed and storage of personal computers, it is no longer necessary to assume the foundation to be a liquid with a fictitious k value. The more realistic solid or layer foundation can be used. The finite element computer program such as ANSYS and ABAQUS based on the finite-element theories and various types of foundations. (Huang, 2004)

3.2 Analytical Methods:

Analytical methods used are either closed form formula or influence charts.

3.2.1 Closed-Form Formulas

These formulas are applicable only to a very large slab with a single wheel load applied near the corner, in the interior of a slab at a considerable distance from any edge, and near the edge far from any corner. The formulas are defined as follows:

a) Corner Loading

As presented by Huang, 2004, the Goldbeck (1919) and Older (1924) formula is the earliest one for use in concrete pavement design. The formula is based on a concentrated load P applied at the slab corner. When a load is applied at the corner, the stress in the slab is symmetrical with respect to the diagonal. For a cross section at a distance x from the corner, the bending moment is Px and the

width of section is 2x. When the subgrade support is neglected and the slab is considered as a cantilever beam, the tensile stress on top of the slab is:

$$\sigma_c = \frac{Px}{\frac{1}{6}(2x)h^2} = \frac{3P}{h^2} \quad (3.1)$$

Huang, 2004 also stated that

Westergaard (1926b) applied a method of successive approximations and obtained the formulas:

$$\sigma_c = \frac{3P}{h^2}\left[1 - \left(\frac{a\sqrt{2}}{l}\right)^{0.6}\right] \quad (3.2)$$

$$\Delta_c = \frac{P}{kl^2}\left[1.1 - 0.88\left(\frac{a\sqrt{2}}{l}\right)\right] \quad (3.3)$$

in which Δc is the corner deflection, l is the radius of relative stiffness, a is the contact radius, and k is the modulus of subgrade reaction .

Ioannides et al. (1985) applied the finite-element method to evaluate Westergaard's solutions. They suggested the use of the relationships:

$$\sigma_c = \frac{3P}{h^2}\left[1 - \left(\frac{c}{l}\right)^{0.72}\right] \quad (3.4)$$

$$\Delta_c = \frac{P}{kl^2}\left[1.205 - 0.69\left(\frac{c}{l}\right)\right] \quad (3.5)$$

in which c is the side length of a square contact area . If a load is applied over a circular area, the value of c must be selected so that the square and the circle have the same contact area:

$$c = 1.772\, a \quad (3.6)$$

b) Interior Loading

As presented by Huang, 2004, the earliest formula developed by Westergaard (1926b) for the stress in the interior of a slab under a circular loaded area of radius a is

$$\sigma_i = \frac{3(1+\mu)P}{2\pi h^2}\left[\ln\left(\frac{l}{b}\right) + 0.6159\right] \quad (3.7)$$

in which l is the radius of relative stiffness and:

$$b = a \text{ when } a \geq 1.724\,h \quad (3.8)$$
$$b = \sqrt{1.6\,a^2 + h^2} - 0.675h \text{ when } a < 1.724\,h \quad (3.9)$$

For a Poisson ratio of 0.15 and in terms of base-10 logarithms, equation (3.7) can be written as:

$$\sigma_i = \frac{0.316P}{h^2}\left[4\log\left(\frac{l}{b}\right) + 1.069\right] \quad (3.10)$$

The deflection equation due to interior loading (Westergaard, 1939) is

$$\Delta_i = \frac{P}{8kl^2}\left[1 + \frac{1}{2\pi}\left[\ln\left(\frac{a}{2l}\right) - 0.673\right]\left(\frac{a}{l}\right)^2\right] \quad (3.11)$$

c) **Edge Loading**

As presented by Huang, 2004, presented of generalized solutions for maximum stress and deflection produced by elliptical and semielliptical areas placed at the slab edge. Setting the length of both major and minor semiaxes of the ellipse to the contact radius a leads to the corresponding solutions for a circular or semicircular loaded area. In the case of a semicircle, its straight edge is in line with the edge of the slab. The results obtained from these new formulas differ significantly from those of the previous formulas. According to Ioannides et al. (1985), the following equations are the correct ones to use:

$$\sigma_{e(\,circle)} = \frac{3(1+\mu)P}{\pi(3+\mu)h^2}\left[\ln\left(\frac{E\,h^3}{100\,k\,a^4}\right) + 1.84 - \frac{4\mu}{3} + \frac{1-\mu}{2} + \frac{1.18(1+2\mu)}{l}\right] \quad (3.12)$$

$$\sigma_{e(\,semicircle)} = \frac{3(1+\mu)P}{\pi(3+\mu)h^2}\left[\ln\left(\frac{E\,h^3}{100\,k\,a^4}\right) + 31.84 - \frac{4\mu}{3} + \frac{(1+2\mu)}{l}\right] \quad (3.13)$$

$$\Delta_{e(\,circle)} = \frac{\sqrt{2+1.2\,\mu\,P}}{\sqrt{Eh^3k}}\left[1 - \frac{(0.76+0.4\mu)a}{l}\right] \quad (3.14)$$

$$\Delta_{e(\,semicircle)} = \frac{\sqrt{2+1.2\,\mu\,P}}{\sqrt{Eh^3k}}\left[1 - \frac{(0.323+0.17\mu)a}{l}\right] \quad (3.15)$$

With the exception of equation for a semicircular loaded area, all of the closed-form formulas presented so far are based on a circular loaded area. When a load is applied over a set of dual tires, it is necessary to convert it into a circular area,

so that the equations based on a circular loaded area can be applied. If the total load is the same but the contact area of the circle is equal to that of the duals, as has been frequently assumed for flexible pavements, the resulting stresses and deflection will be too large. Therefore, for a given total load, a much larger circular area should be used for rigid pavements, Figure 3.1 shows a set of dual tires and the area of each tire is

$$\frac{Pd}{q} = \pi(0.3\,L)^2 + (0.4\,L)\,(0.6L) = 0.28326L^2 + 0.24L^2 = 0.5227L^2 \qquad (3.16)$$

$$L = \sqrt{\frac{Pd}{0.5227q}} \qquad (3.17)$$

The area of an equivalent circle is:

$$\pi\,a^2 = 2 \times 0.5227L^2 + (Sd - 0.6L)L = 0.4454\,L^2 + Sd_L L \qquad (3.18)$$

$$\pi a^2 = \frac{0.8521\,Pd}{q} + Sd\sqrt{\frac{Pd}{0.5227q}} \qquad (3.19)$$

So the radius of contact area is:

$$a = \sqrt{\left(\frac{0.8521\,Pd}{q\pi} + \left(\frac{Sd}{\pi}\left(\frac{Pd}{0.5227q}\right)\right)^{0.5}\right.} \qquad (3.20)$$

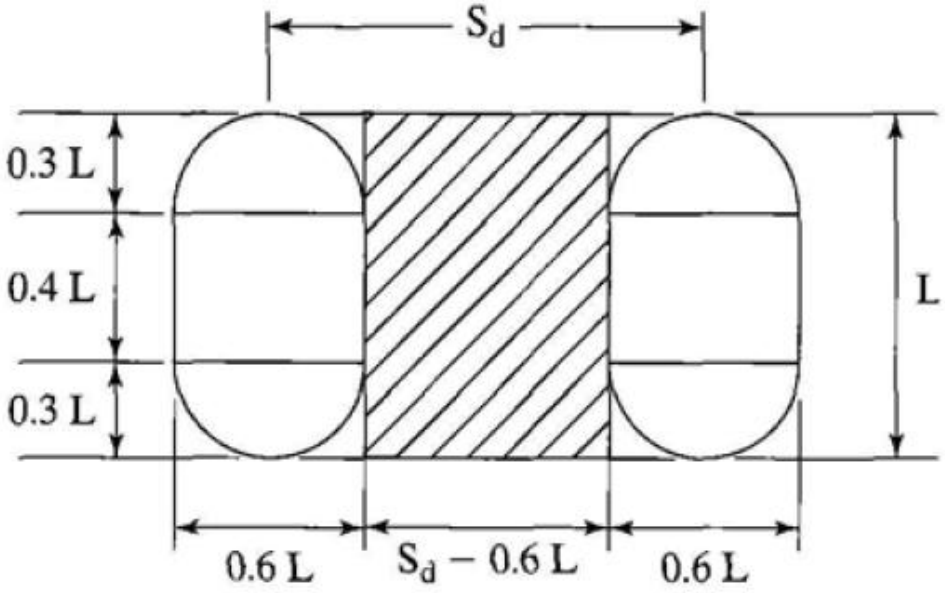

Figure 3.1 set of dual tires(Huang,2004)

3.2.2 Influence Charts

As presented by Huang, 2004,

influence charts based on liquid foundations (Pickett and Ray, 1951) were used previously by the Portland Cement Association for rigid pavement design. The charts are based on Westergaard's theory with a Poisson ratio of 0.15 for the concrete slab. Only charts for interior and edge loadings are available, the interior loading being used for the design of airport pavements (PCA, 1955) and the edge loading for the design of highway pavements (PCA, 1966). (Huang, 2004)

Interior Loading

Figure 3.2 shows the applications of influence charts for determining the moment at the interior of slab. The moment is at point 0 in the n direction. To use the chart, it is necessary to determine the radius of relative stiffness l presented in the following equation:

$$l = \left[\frac{E\,h^3}{12(1-\mu^2)k}\right]^{0.25} \tag{3.21}$$

By counting the number of blocks N covered b y the tire imprints, the moment in the n direction M can be determined from:

$$M = \frac{ql^2N}{10000} \tag{3.22}$$

The stress is determined by dividing the moment by the section modulus:

$$\sigma i = \frac{6M}{h^2} \tag{3.23}$$

For the tire imprints shown in Figure 3.2, the moment is under the center of the lower left tire in the lateral direction. If the moment in the longitudinal direction is desired, the tire assembly must rotate 90° clockwise so that two of the tires lie in the zone of negative blocks, and the moment becomes much smaller. Figure 3.3 shows the influence chart for deflection due to interior loading. The chart is axisymmetric, and the blocks are formed by concentric circles and radial lines. The deflection is at the center of the circles. The use of the chart is similar to that of Figure 3.3. After the number of blocks covered by the tire imprint is counted, the deflection can be determined as:

$$\Delta i = \frac{0.0005q\ l^4 N}{D} \tag{3.24}$$

$$D = \frac{Eh^3}{12(1-\mu^2)} \tag{3.25}$$

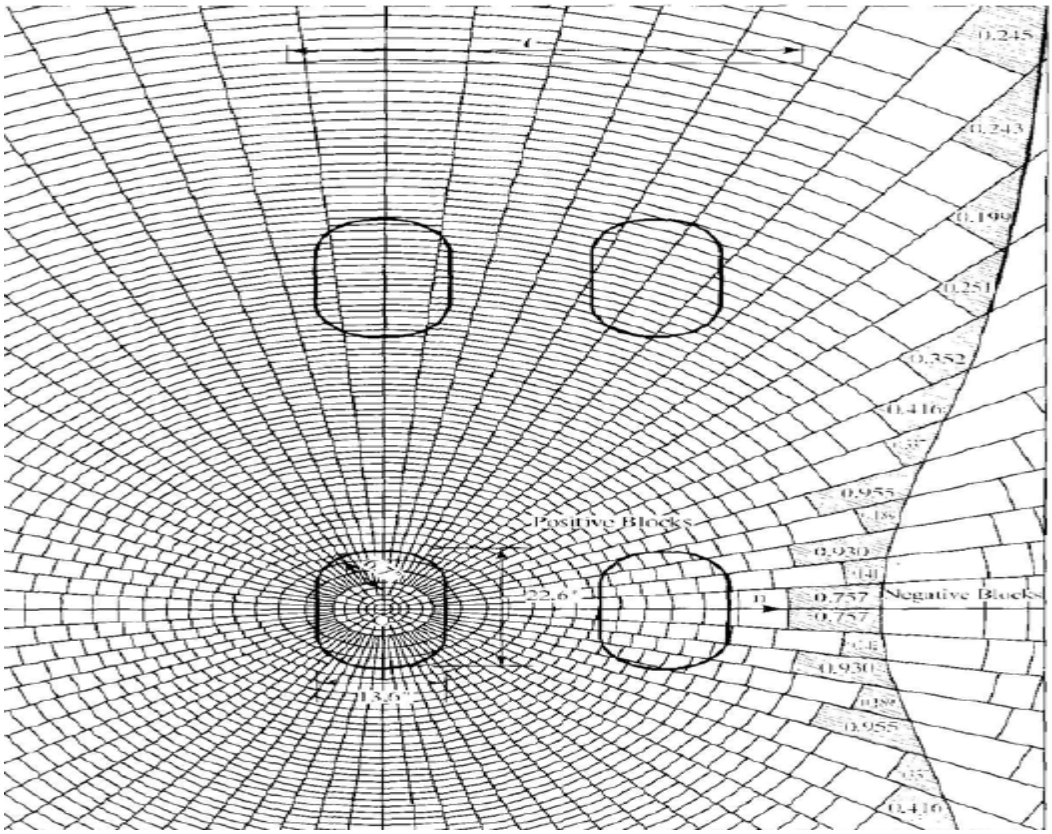

Figure 3.2 Application of influence chart for determining moment (1 in. = 25 .4 mm). (Huang, 2004).

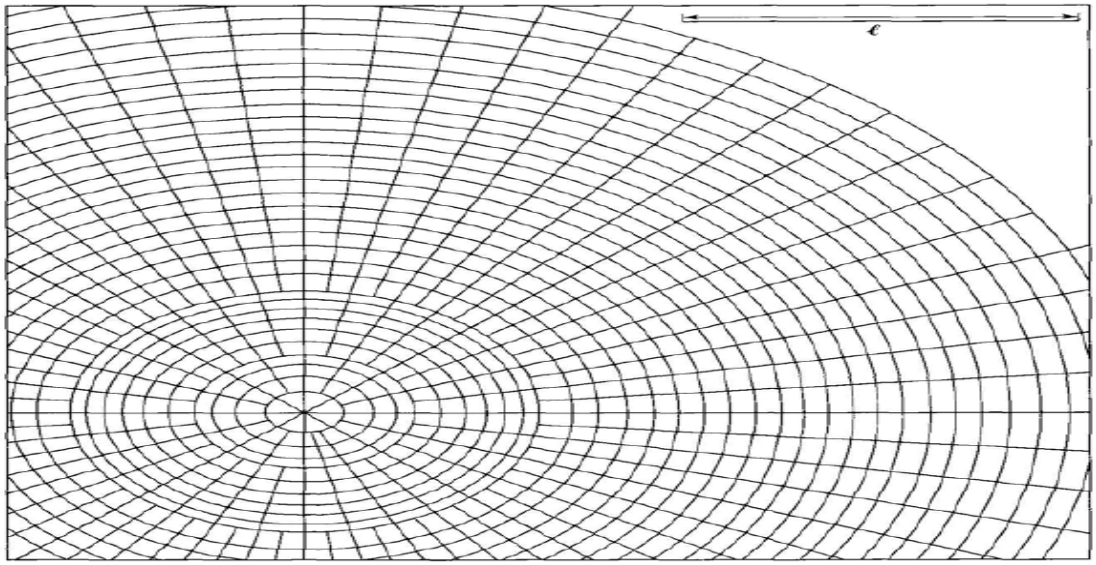
Figure 3.3 Influence chart for deflection due to interior loading. (Huang, 2004)

3.3 Numerical Methods:

3.3.1 Basic Introduction:

The analysis of stress and deformation of the loading of simple geometric structures can usually be accomplished by closed-form techniques. As the structures become more complex, the analyst is forced to use approximations of closed-form solutions, experimentation, or numerical methods. There are a great many numerical techniques used in engineering applications for which digital computers are very useful. In the field of structural analysis, the numerical techniques generally employ a method which discretizes the continuum of the structural system into a finite collection of points (or nodes)/ elements called finite elements. The most popular technique used currently is the finite element method (FEM). Other methods include trial functions via variational methods and weighted residuals, the finite difference method (FDM), structural analogues, and the boundary element method (BEM). Some of the main numerical methods are outlined as follows:

3.3.2 The Finite Difference Method (FDM)

In the field of structural analysis, one of the earliest procedures for the numerical solutions of the governing differential equations of stressed continuous solid bodies was the finite difference method. In the finite difference approximation of differential equations, the derivatives in the equations are replaced by difference quotients of the values of the dependent variables at discrete mesh points of the domain. After imposing the appropriate boundary conditions on the structure, the discrete equations are solved obtaining the values of the variables at mesh points. The technique has many disadvantages, including inaccuracies of the derivatives of the approximated solution; difficulties in imposing boundary conditions along curved boundaries, difficulties in utilizing non-uniform and non-rectangular meshes.

3.3.3 The Boundary Element Method (BEM)

The boundary element method developed more recently than FEM, transforms the governing differential equations and boundary conditions into integral equations, which are converted to contain surface integrals. Because only surface integrals remain, surface elements are used to perform the required integrations. This is the main advantage of BEM over FEM, which require three-dimensional elements throughout the volumetric domain. Boundary elements for a general three dimensional
solid are quadrilateral or triangular surface elements covering the surface

area of the component. For two-dimensional and axisymmetric problems, only line elements tracing the outline of the component are necessary.

Although BEM offers some modelling advantages over FEM, the latter can analyze more types of engineering applications and is much more firmly entrenched in today's computer-aided-design (CAD) environment.

3.3.4 Finite Element Method (FEM)

3.3.4.1 Basic Concept

Finite Element Method (FEM) was first developed in 1943 by R. Courant, who utilized the Ritz method of numerical analysis and variation calculus to obtain approximate solutions to vibration systems. The finite element method is a numerical procedure that can be applied to obtain approximate solutions to a variety of problems in engineering. Steady, transient, linear, or nonlinear problems in stress analysis, heat transfer, fluid flow, and electromagnetism problems may be analyzed with the finite element method

In the finite element method of analysis, a complex region defining a continuum is discretized into simple geometric shapes called finite elements. The material properties and the governing relationships are considered over these elements and expressed in terms of unknown values at elements corners. An assembly process duly considering the loading and constraints results in a set of equations. Solution of these equations gives the approximate behavior of the continuum

3.3.4.2 Basic steps in the Finite Element Displacement Method

The following are the steps adopted for analyzing a structural engineering problem by the finite element method:

1. **Discretization of the domain**

The continuum is divided into a number of finite elements by imaginary lines or surfaces. The interconnected elements may have different sizes and shapes. The choice of the simple elements or higher order element straight or curved, it's shape, refinement are to be decided before the mathematics formulation starts.

2. **Identification of variables**

The elements are assumed to be connected at their intersecting points referred to as nodal points. At each node, generalized displacements are the unknown degrees of freedom.

3. Choice of approximating functions

Once the variables and local coordinate system have been chosen. The next step is the choice of displacement function. This function represents the variation of the displacements within the element. The function can be approximated in a number of ways. The displacement function may be approximated in the form of
a linear function or a higher order function. The shape of element or the geometry may also be approximated. The coordinates of corner nodes define the element shape accurately if the element is actually made of straight line or plates.

4. Formation of the element stiffness matrix

After the continuum is discretized with desired element shapes, the element stiffness matrix is formulated. With the exception of a few simple elements, the element stiffness matrix for majority of elements is not available in explicit form. As such they require numerical integration for their evaluation. The geometry of the element is defined in reference to a global frame. In many problems such as those of rectangular plates, the global and local axis systems are coincident and for them no further calculation is needed at the element level beyond computation of element stiffness matrix in local coordinates. Coordinates transformation must be done for all elements where it is needed.

5. Formulation of the overall stiffness matrix

After the element stiffness matrices in the global coordinates are formed, they are assembled to form the overall stiffness matrix. The assembly is done through the nodes, which are common to adjacent elements. At the nodes, the continuity of the displacement function and possibly their derivatives are established. The overall stiffness matrix is symmetric and banded.

6. Incorporation of boundary conditions

The boundary restraint conditions are to be imposed in the overall stiffness matrix. There are various techniques available to satisfy the boundary conditions. In some of these approaches, the size of the stiffness matrix may be reduced or condensed in its final form. To ease the computer programming

aspect and to elegantly incorporate the boundary conditions, the size of the overall stiffness matrix is kept the same.

7. Formulation of element load matrix

The loading inside the element is transferred at the nodal points and consistent element load matrix is formed. Sometimes, based on the typicality of problem, the load matrix may be simplified.

8. Formation of the overall load matrix

Like the overall stiffness matrix, the element loading matrices are assembled to the vector of concentrated nodal loads form the overall loading matrix. This matrix has one column per loading case and it is either a column vector or a rectangular matrix depending on the number of loading conditions.

9. Solution of simultaneous conditions

All the equations required for the solution of the problem are now developed. In the displacement method, the unknowns are the nodal displacements. The gauss elimination and Cholesky's factorization are the most commonly used procedures for the solution of simultaneous equations. These methods are well suited to a small or moderate number of equations. For large sized problems, a frontal technique is one of the methods of obtaining solution. For systems of large order, Gauss-Seidel or Jacobi iterations are more suited

10. Calculation of stress or stress-resultants

In the previous step, nodal displacements are calculated and these values are utilized for the calculation of stresses or stress-resultants. This may be done for all elements of the continuum or it may be limited only to some predetermined elements. Results may be obtained by graphical means. It may be desirable to plot the contour of the deformed shape of the continuum. The contour of the principal stresses may be one of the sought after items for certain category of problems.

3.3.4.3Three Dimensional Element

a) Basic Finite Element Relationships

The basic steps are the derivation of the element stiffness matrix, which relate the nodal displacement vector $\{d\}$ to the nodal force vector $\{f\}$ are described below.

Considering a body subjected to a set of external forces, the displacement vector at any point within the element $[u]^{\mathrm{e}}$ is given by

$$\{u\}^e = [N][d]^e \tag{3.26}$$

Where, [N] is the matrix of shape functions, $[d]^{\mathrm{e}}$ the column vector of nodal displacements.

The strain at any point can be determined by differentiating the displacement vector as:

$$\{\varepsilon\}^e = [L][u]^e \tag{3.27}$$

Where, [L] is the matrix of differential operator. In expanded form, the strain vector can be expressed as:

$$\{\varepsilon\} = \begin{Bmatrix} \varepsilon x \\ \varepsilon y \\ \varepsilon z \\ \gamma xy \\ \gamma yz \\ \gamma zx \end{Bmatrix} = \begin{Bmatrix} \frac{\partial u}{\partial x} \\ \frac{\partial v}{\partial y} \\ \frac{\partial w}{\partial z} \\ \frac{\partial u}{\partial y} + \frac{\partial v}{\partial x} \\ \frac{\partial v}{\partial z} + \frac{\partial w}{\partial y} \\ \frac{\partial w}{\partial x} + \frac{\partial u}{\partial z} \end{Bmatrix} \tag{3.28}$$

Substituting from equation displacement into strain gives:

$$\{\varepsilon\}^e = [\mathrm{B}]\{\mathrm{d}\}^e \tag{3.29}$$

Where, [B] is strain-nodal displacements matrix given by:

$$[\mathrm{B}] = [\mathrm{L}]\,[N] \tag{3.30}$$

The stress vector can be determined by using the appropriate stress-strain relationship as:

$$\{\sigma\}^e = [D]\{\varepsilon\}^e \tag{3.31}$$

From the above equations, the stress-nodal displacement relationship can be expressed as:

$$\{\sigma\}^e = [D][B]\{\mathrm{d}\}^e \tag{3.32}$$

b) Eight-Noded Solid Element

3-D concrete solid is used for the 3-D modelling of solids with or without fibers. The solid is capable of cracking in tension and crushing in compression. In concrete applications, for example, the capability of the solid element may be used to model the concrete, while the rebar capability is available for modelling fiber behavior. The element is defined by eight nodes having three degrees of freedom at each node: translations of the nodes in x, y and z-directions. The element is bounded by six quadrilateral faces and has eight nodes. The geometry of the element is described by the Cartesian coordinates (xi,yi,zi)) of the eight nodes each node i has three degrees of freedom (ui,wi , vi). Figure 3.4 Solid 3D concrete element Fig. 3.4(a) shows an eight noded element with node numbering and the natural coordinates.

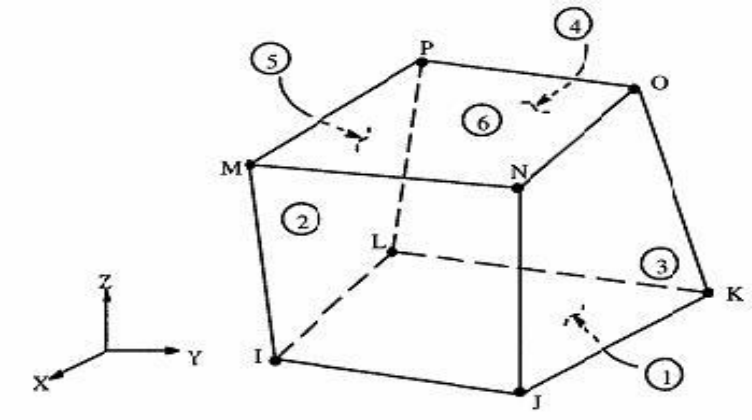

Figure 3.4 (a)Solid 3D concrete element

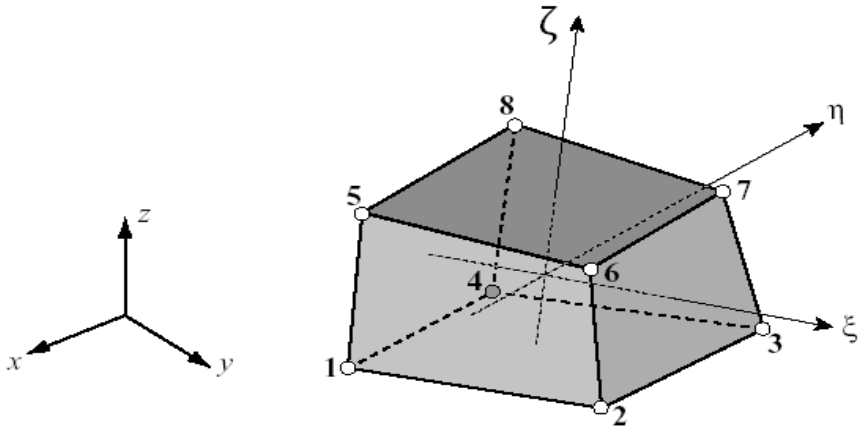

Figure 3.4 (b) 8-node hexahedron and the natural coordinate's ξ, η, μ

The displacement can be expressed as

$$\{u\} = [N]\{q\} \tag{3.33}$$

Where, [N] is the matrix of shape functions

$$[N] = \begin{bmatrix} \boldsymbol{N1} & \mathbf{0} & \mathbf{0} & \boldsymbol{N2} & \mathbf{0} & \mathbf{0} & \cdots & \boldsymbol{N8} & \mathbf{0} & \mathbf{0} \\ \mathbf{0} & \boldsymbol{N1} & \mathbf{0} & \mathbf{0} & \boldsymbol{N2} & \mathbf{0} & \cdots & \mathbf{0} & \boldsymbol{N8} & \mathbf{0} \\ \mathbf{0} & \mathbf{0} & \boldsymbol{N1} & \mathbf{0} & \mathbf{0} & \boldsymbol{N2} & \cdots & \mathbf{0} & \mathbf{0} & \boldsymbol{N8} \end{bmatrix} \tag{3.34}$$

{q} = the column vector of nodal displacements i.e.(Xi, Yi, and Zi are displacement components of node i.

Element strain matrix

can be written as

$$\{\varepsilon\} = \{B\}\ \{q\} \tag{3.35}$$

Where

$$[B] = \begin{bmatrix} \frac{\partial N1}{\partial x} & 0 & 0 & \frac{\partial N2}{\partial x} & 0 & 0 & - - - & \frac{\partial N8}{\partial x} & 0 & 0 \\ 0 & \frac{\partial N1}{\partial y} & 0 & 0 & \frac{\partial N2}{\partial y} & 0 & - - - & 0 & \frac{\partial N8}{\partial y} & 0 \\ 0 & 0 & \frac{\partial N1}{\partial z} & 0 & 0 & \frac{\partial N2}{\partial z} & - - - & 0 & 0 & \frac{\partial N8}{\partial z} \\ \frac{\partial N1}{\partial y} & \frac{\partial N1}{\partial x} & 0 & - & - & - & - - & \frac{\partial N8}{\partial y} & \frac{\partial N8}{\partial x} & 0 \\ 0 & \frac{\partial N1}{\partial z} & \frac{\partial N1}{\partial y} & - & - & - - - - & & 0 & \frac{\partial N8}{\partial z} & \frac{\partial N8}{\partial y} \\ 0 & 0 & \frac{\partial N1}{\partial z} & - & - & - - - - & & \frac{\partial N8}{\partial z} & 0 & \frac{\partial N8}{\partial x} \end{bmatrix} \quad (3.36)$$

Element stress

The stresses σ at any point with in the HEXA 8 element are evaluated using

$\{\sigma\} = [D]\,[B]\,\{q\} - [D]\{g\}^{initi}$ (3.37)

Where the $\{g\}^{initi}$ is the initial strains due to thermal expansion

Element stiffness matrix

$[k] = \int [B]^{T}[D]\,[B]\,dv_e$ (3.38)

c) 3D Plate Finite Element:

A plate is a three dimensional solid body with one of the plate dimensions much smaller than the other two, zero curvature of the plate mid-surface in the reference configuration and loading that causes bending deformation and shell is a three dimensional solid body with one of the shell dimensions much smaller than the other two, non-zero curvature of the shell mid-surface in the current configuration and loading that causes bending and stretching deformation. Table 3.1 shows the several different plate theories. and figure 3.5 (a & b) shows the thin finite plate element.

Figure 3.5 (a)

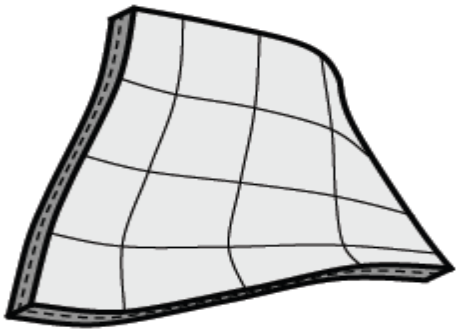

Figure 3.5 (b)

Figure 3.5 Plate and Shell finite element three dimensional (cirak, F., 2016)

Table 3.1 several different plate theories (Cirak, F., 2016).

	Thick	thin	very thin
Length/ thickness	5 to 10	10 to 100	> 100
physical characteristics	transverse shear deformations	Negligible transverse shear deformations	geometrically nonlinear

For the thin rectangular plate element (Huang, 2016) Figure 3.6 shows a rectangular finite element with nodes i, j, k, and 1. At each node there are three fictitious forces and three corresponding displacements. The three forces are a vertical force Fw, a moment about the x axis Fθx, and a moment about the y axis Fθy. The three displacements are the vertical deflection in the z direction w, a rotation about the x axis θx, and a rotation about the y axis θy . The positive direction of the coordinates is shown in the figure and the positive direction of moments and rotations can be determined by the right-hand rule. For each element, the forces and displacements are related by:

$$\begin{bmatrix} Fi \\ Fj \\ Fk \\ Fl \end{bmatrix} = [Kp]^e \begin{bmatrix} \delta i \\ \delta j \\ \delta k \\ \delta l \end{bmatrix} \tag{3.39}$$

in which$[Kp]^e$ is the element stiffness matrix of a plate. At any given node,

$$Fi = \begin{bmatrix} Fw_i \\ F\theta_{xi} \\ F\theta_{yi} \end{bmatrix} \tag{3.40}$$

$$\delta i = \begin{bmatrix} w_i \\ \theta_{xi} \\ \theta_{yi} \end{bmatrix} \tag{3.41}$$

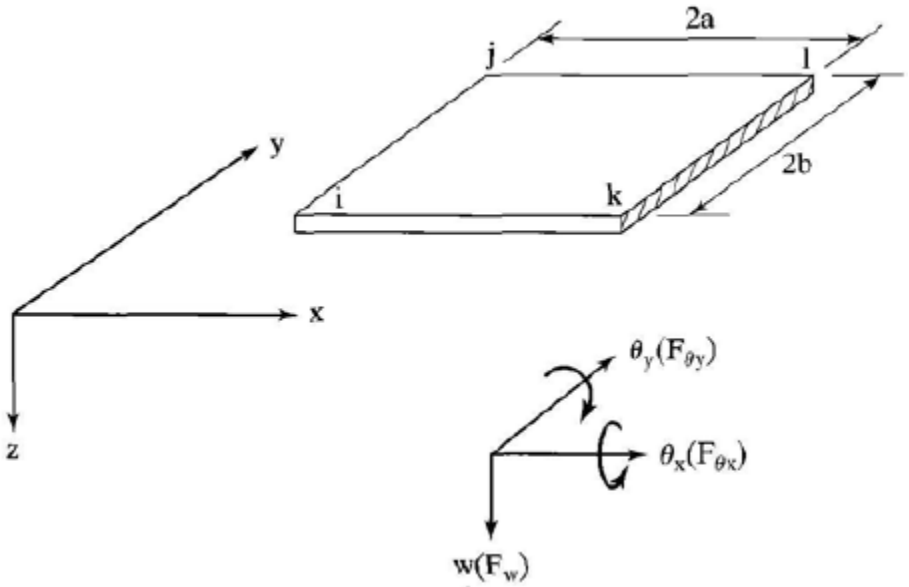

Figure 3.6 A thin rectangular plate element. (Huang, 2004).

3.3.4.4 Foundations under Slab Finite Element (Huang, 2004):

Three different types of pavement foundation can be assumed: elastic, solid, and layer. Westergaard's theory and most of the finite element computer programs in use today are based on the liquid foundation. The use of liquid foundations results in a banded matrix for the simultaneous equations and requires very little computer time to solve. However, with the much faster speed and larger storage of personal computers, the more realistic solid and layer foundations should be used, if needed. The liquid foundation is also called a Winkler foundation, with the force deflection relationship characterized by an elastic spring. The term "liquid" does not mean that the foundation is a liquid with no shear strength, but simply implies that the deformation of the foundation under a slab is similar to that of water under a boat. According to Archimedes' principle, the weight of the boat is equal to the weight of water displaced. This is similar to the case where a slab is placed on an infinite number of springs and the total volume of displacement is proportional to the total load applied. The stiffness of a liquid foundation is defined by:

$$k = \frac{p}{\Delta} \tag{3.42}$$

in which k is the modulus of subgrade reaction; p is the unit pressure, or force per unit area; and w is the vertical deflection. for the subgrade, k can range from 50 to 800 pci. Figure 3.4 shows the replacement of the large number of springs under a rectangular plate element, with a length of 2a and a width of 2b, by four identical springs at the corners. The force on each spring is equal to the unit pressure p multiplied by the area a ×b. the force at node i, Fwi , is related to the deflection
at node i, wi, by

$$Fwi = Kabwi \tag{3.43}$$

Equation 3.44 can be applied directly when the node is located at the corner of a slab. If the node is located at the edge or interior of a slab, superposition of two or four adjoining elements is required to obtain the force displacement relationship.

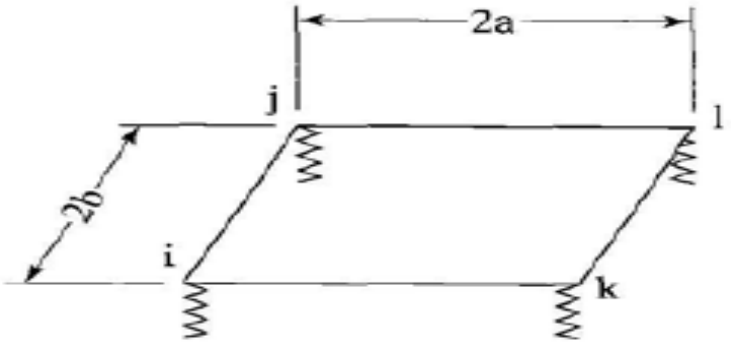

FIGURE 3.7 elastic foundations under a plate element (Huang, 2004).

3.3.4.6 Slab–Subgrade Contact (Huang, 2004)

An important factor that affects the design of concrete pavements is the contact condition between slab and foundation. Both Westergaard's analysis for liquid foundations and Pickett's analysis for solid foundations are based on the assumption that the slab and foundation are in full contact. This assumption is valid if there are no gaps between slab and foundation, because the weight of the slab naturally imposes a large pre compression on the foundation, which will keep the slab and foundation in full contact. However, this is not true when the slab is subjected to curling or pumping, which results in a separation between slab and foundation.

3.3.5 ANSYS Program Descriptions (Bourde,G., 2017)

The ANSYS computer program is based on the finite-element method, in which the slab is divided into rectangular finite elements with a large number of nodes. Both wheel loads and subgrade reactions are applied to the slab as vertical concentrated forces at the nodes and ANSYS is useful to final element simulations for pavement uses SOLID for pavement, CONTA 174 and TARGE 173 to define contact between them.

a) SOLID186 Element Description

SOLID186 is a higher order 3-D 20-node solid element that exhibits quadratic displacement behavior. The element is defined by 20 nodes having three degrees of freedom per node: translations in the nodal x, y, and z directions. The element supports plasticity, hyper elasticity, creep, stress stiffening, large deflection, and large strain capabilities. It also
has mixed formulation capability for simulating deformations of nearly incompressible elastoplastic materials, and fully incompressible hyper elastic materials.

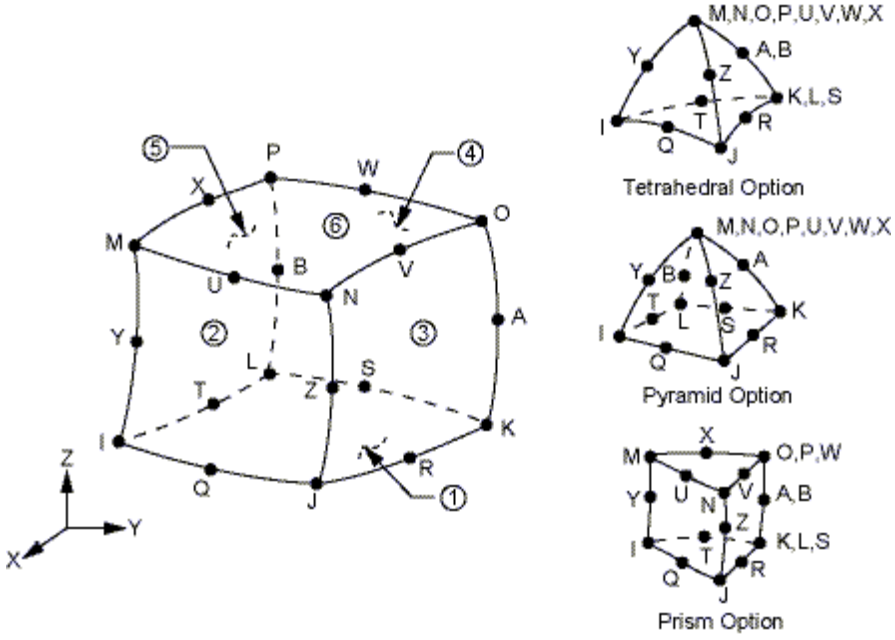

Figure 3.8 SOLID186 homogenous structural solid geometry (ANSYS manual, 2015)

b) CONTA174 and TARGE170

The 3-D contact surface elements (CONTA173 and CONTA174) are associated with the 3-D target segment elements (TARGE170) via a shared real constant set. ANSYS looks for contact only between surfaces with the same real constant set. For either rigid-flexible or flexible-flexible contact, one of the deformable

surfaces must be represented by a contact surface. Real constant R1 is used only to define the radius if the associated target shape (TARGE170) is a cylinder, cone, or sphere. Real constant R2 is used to define the radius of a cone end at the second node.

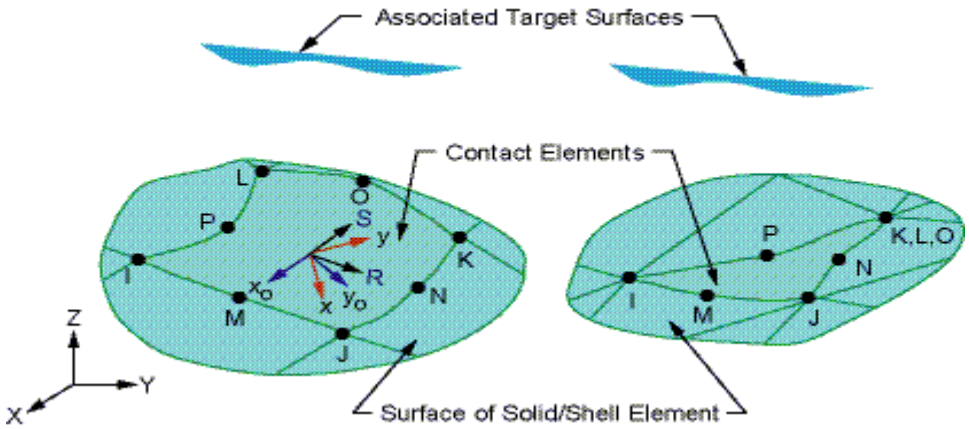

Figure 3.9 CONTA174 and TARGE170 for solid and shell element (ANSYS manual, 2015)

CHAPTER FOUR
RESULTS AND DISSCUSION

4.1 Analysis and Design Data:

4.1.1 General description of case study:

The data of design of rigid pavement of JFKIA constructed in August 2010, obtained from F.A.A report study of "review of concrete airport pavement presented in international conference on best practices for concrete pavements shows in Appendix (B) includes projects, single slab test, typical strain responses, critical stress and FAARFIELD model. Table 4.1 shows the typical of several aircrafts and Table 4.2 shows the Contact area for different tire imprint.

Table 4.1 Data for Several Typical Aircrafts. (Yoder and Witzak 1975)

Type of plane	Max Gross Weight (Ib×10^3)	Type of Gear	Main Gear Dimension (in)	Max Load Each Main Assembly (Ib×10^3)	Tire Pressure (psi)
Boeing 707-320C	**336.0**	**Twin-Tandem**	**56×34.5**	**157.0**	**180**
Boeing 707-120B	**258.0**	**Twin-Tandem**	**56×34**	**120.0**	**170**
Boeing 737	**111.0**	**Twin**	**30.5**	**25.8**	**148**
Boeing727-100	**170.0**	**Twin**	**34.0**	**76.9**	**166**
Boeing747	**713.0**	**Double Twin-Tandem**	**58×44**	**166.5**	**204**
McDonnel-Douglas DC10-10	**413.0**	**Twin-Tandem**	**54×64**	**194.0**	**177**
McDonnel-Douglas DC8-43	**318.0**	**Twin-Tandem**	**55×30**	**148.0**	**127**
McDonnel-Douglas DC9-15	**91.0**	**Twin**	**24**	**42.4**	**174**

Table 4.2 Contact area for different tire imprint (Rehman etal, 2011)

Imprint shape	Wheel pressure (MPa)	Contact area (sq. mm)
Circular	**0.67**	**60000**
Rectangular	**0.67**	**61575**
Ellipse	**0.67**	**60416**
Actual	**0.67**	**60318**

For the analysis and selection of the appropriate contact area, same tire pressure is applied for different imprint shape of equal contact area and thus the effect of maximum principal stresses and strains are measured. Tire contact dimension is selected from the suggested rules of PCA method, that is circular, rectangular or ellipsoid area which is equivalent to actual contact area and difference in stresses and strains are observed.

The materials of rigid pavements consist of slabs of Portland cement concrete placed on a subbase that is supported on a compacted subgrade. Like flexible pavements, a properly designed rigid pavement provides a nonskid surface which prevents the infiltration of water into the subgrade, while providing structural support to aircraft which use the pavement. The subbase under rigid pavements provides uniform stable support for the concrete slabs. As a rule, a minimum thickness of 4 (in) is required for all subbases under rigid pavements. There are various types of mixtures which are acceptable for rigid pavement subbases including:

Item P-154—Subbase Course

Item P-208—Aggregate Base Course

Item P-209—Crushed Aggregate Base Course

Item P-211—Lime Rock Base Course

Item P-301—Soil Cement Base

Item P-304—Cement Treated Base Course

Item P-306—Econocrete Subbase Course

Item P-401—Plant Mix Bituminous Pavements

Item P-403—HMA Base Course

For rigid pavements accommodating aircraft greater than 100,000 lb maximum gross weight a stabilized subbase is required, which include items P-304, P-306, P-401, and P-403.

In this study, an approach being made to establish the proper tire configuration, tire, contact area and inflation pressure using the traditional methods and 3D finite element software "ANSYS" to analyze stresses and deflection behavior of airport rigid pavement regarding the application of finite element in design purpose. Stresses and deflection are used more and more to predict pavement distresses, and thus the relative condition of the various layers in the pavement structure, the constitutive relationship of stress and deflection in FEM is required to understand and Review the state of art of airport rigid pavement response models for characterization of stresses and deflection and elucidate the importance to improve the stress prediction to prevent premature failure caused by loading and pavement layers.

4.2 predictions of stress and deflection in J.F Kennedy runway pavement using analytical model:

4.2.1 Design Data and Properties

A runway concrete pavement is of size 120 in ×120 in having thickness h = 12 in, load is having circular contact area of radius = 13.5 in and load applied on a circular area p = 166.5 ksi , foundation stiffness k = 165 psi a modulus of elasticity and Poisson ratio is 4000000 psi and 0.15 respectively and calculated radius of relative stiffness l = 43.47 in . a pavement is analyzed by Westergaard closed form solution. Figure (4.1) shows the configuration for interior loading and table 4.3 shows the result of stress and deflection according to interior case of slab.

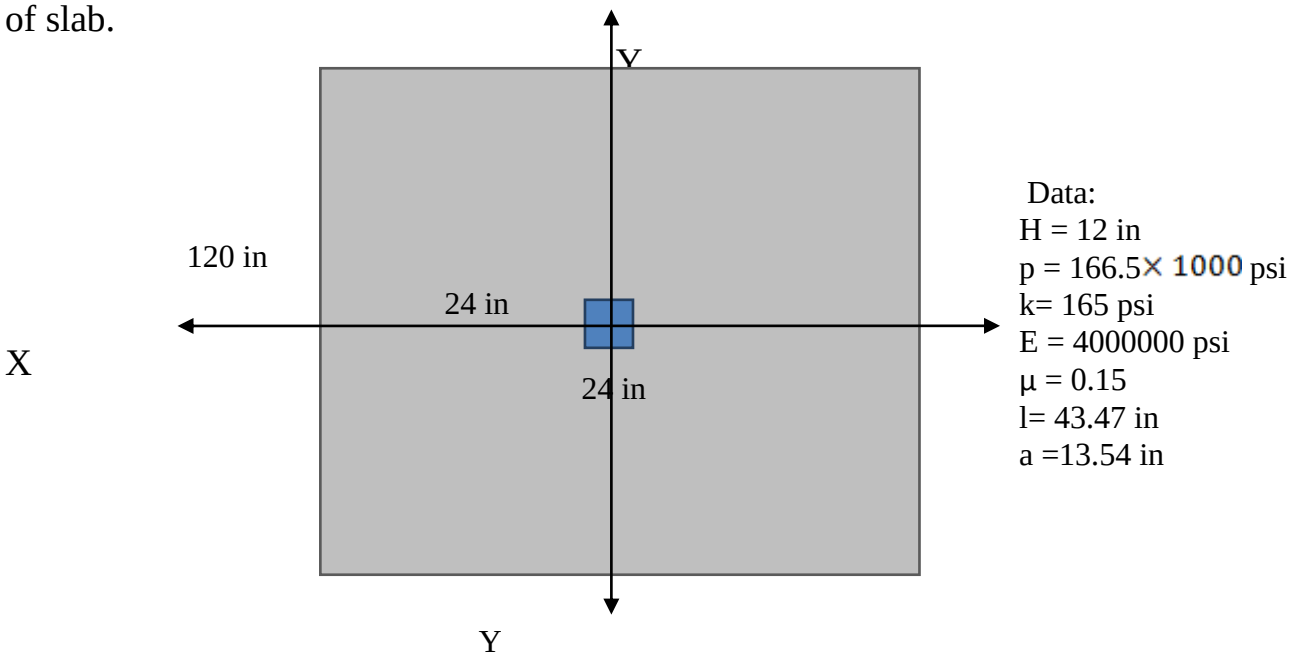

Figure (4.1) System configuration of interior loading. (F.A.A, 1998)

For the runway statement uses the Westergaards theory in interior case. For both stress and deflection

4.2.2 Stress Analysis:

Step (1): calculate stress equation parameters from given design data of JFKIA:

b= $\sqrt{1.6\ a^2 + \ h^2}$ - 0.675 h = $\sqrt{1.6\ 13.5^2 + \ 12^2}$ - 0.675 (12) = 12.81

$$l = \left[\frac{E\ h^3}{12(1-\mu^2\ )k}\right]^{0.25} = \left[\frac{4000000\ 12^3}{12(1-0.15^2\ )165}\right]^{0.25} = 43.47\ in$$

Step (2) Stress Calculation

By using Eq 3.10:

$$\sigma_i = \frac{0.316P}{h^2}\left[4\log(\frac{l}{b}) + 1.069\right] = \frac{0.316(166500)}{12^2}\left[4\log(\frac{43.47}{12.81}) + 1.069\right]$$
$$= 775.003 \text{ psi}$$

4.2.3 Deflection analysis:

By using Eq 3.11

$$\Delta_i = \frac{P}{8kl^2}\left[1 + \frac{1}{2\pi}\left[\ln\left(\frac{a}{2l}\right) - 0.673\right]\left(\frac{a}{l}\right)^2\right]$$

$$= \frac{166500}{8(165)(43.47)^2}\left[1 + \frac{1}{2\pi}\left[\ln\left(\frac{13.54}{2(43.47)}\right) - 0.673\right]\left(\frac{13.54}{43.47}\right)^2\right] = 0.0679457 \text{ in}$$

Table 4.3 stresses and deflection results using analytical method

Method	Stresses (psi)	Deflection (in)
Westergaards solution	775.003	0.0679457

4.2 Finite Element Analysis Model Result

4.2.1 Design data and properties

The model of airport concrete plate is of size 120 inch ×120 inch having thickness 12 inch is created in static structure analysis in ANSYS. A load of

166.5 ksi having circular contact area of radius a=13.54 (in) is applied on the plate. Foundation for plate is modelled as elastic foundation (Spring foundation) having foundation stiffness k=165 psi and modulus of elasticity is 4000000 and Poisson's ratio is 0.15 respectively and the friction ratio Slab/Foundation was taken equal to 1.5. All the edges of pavement are infinite edges due to Westergaard theory assumptions. 8 noded tetrahedron element is used to model the pavement. Figure (4.2) shows airport pavement model. The report of ANSYS program include units, model geometry and coordinate system and materials data shows in appendix (A).

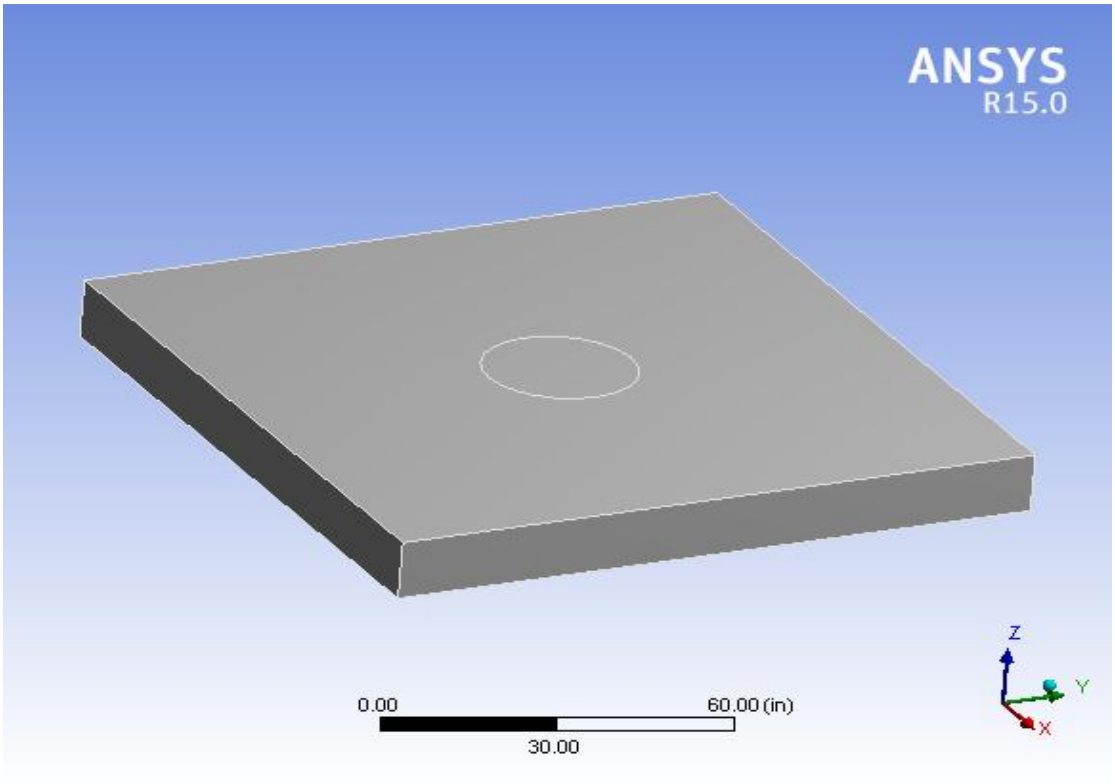

Figure (4.2) Pavement model of size 120 in× 120 in

Figure (4.3) shows interior loading position where load is applied. Figure (4.4) meshing of pavement model, Figure (4.5) stresses developed in the pavement due to interior loading and Figure (4.6) deflection that occurred in the pavement and maximum deflection is under the load patch.

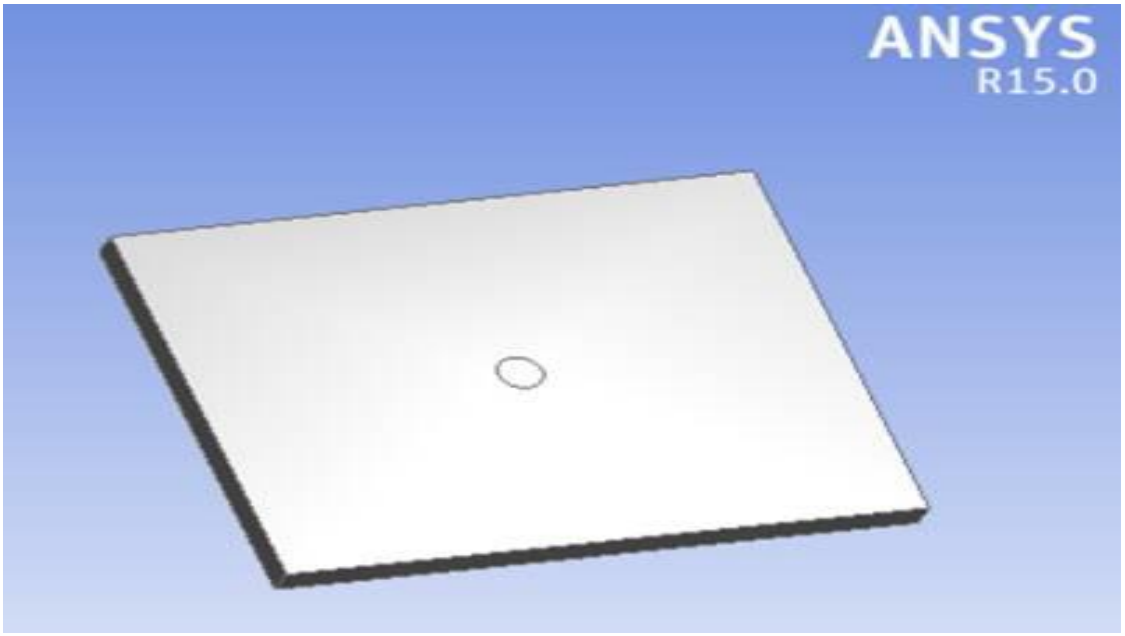

Fig (4.3) interior loading position where load is applied.

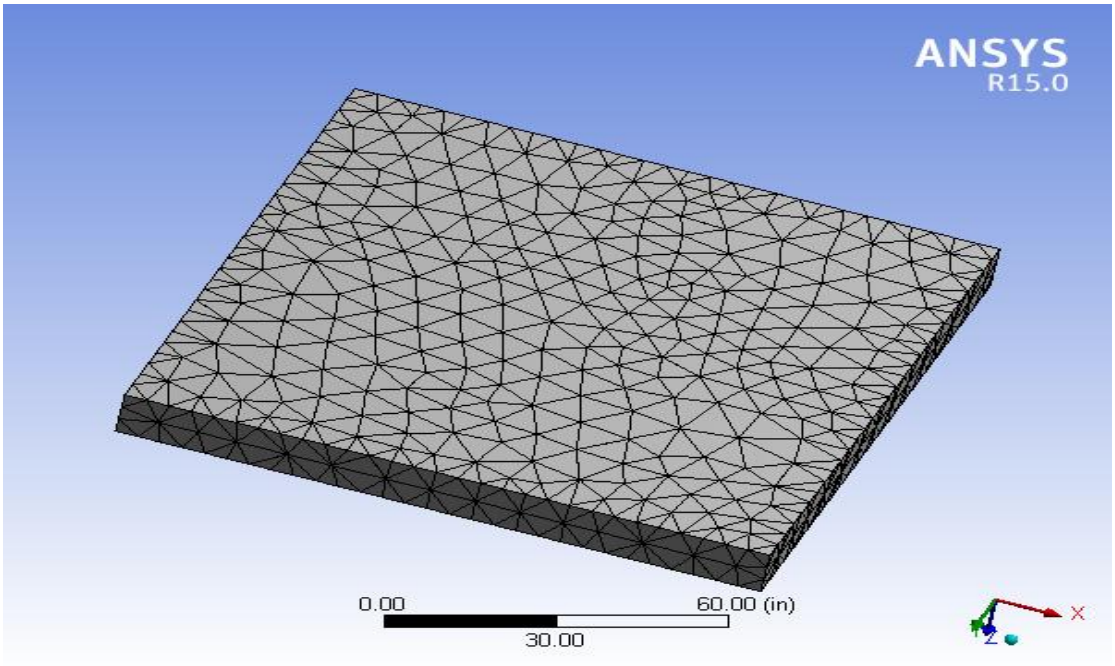

Figure (4.4) meshing of pavement model

4.2.2 Finite Element Model result:

a) Stress Analysis:

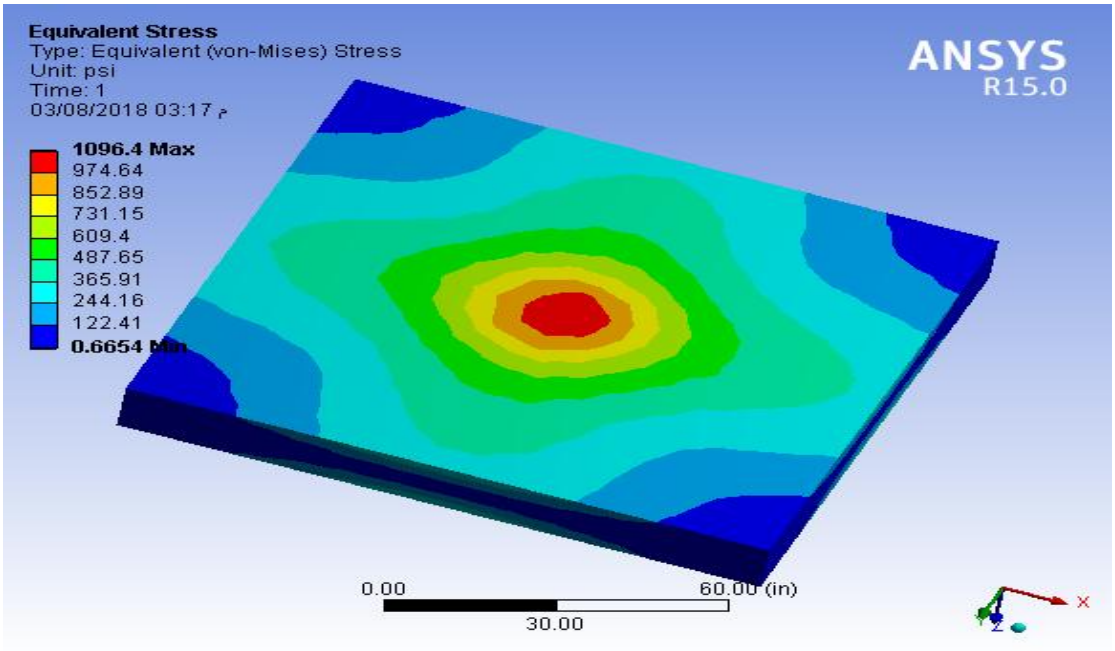

Figure (4.5) stresses developed in the pavement due to interior loading

b) Deflection Analysis:

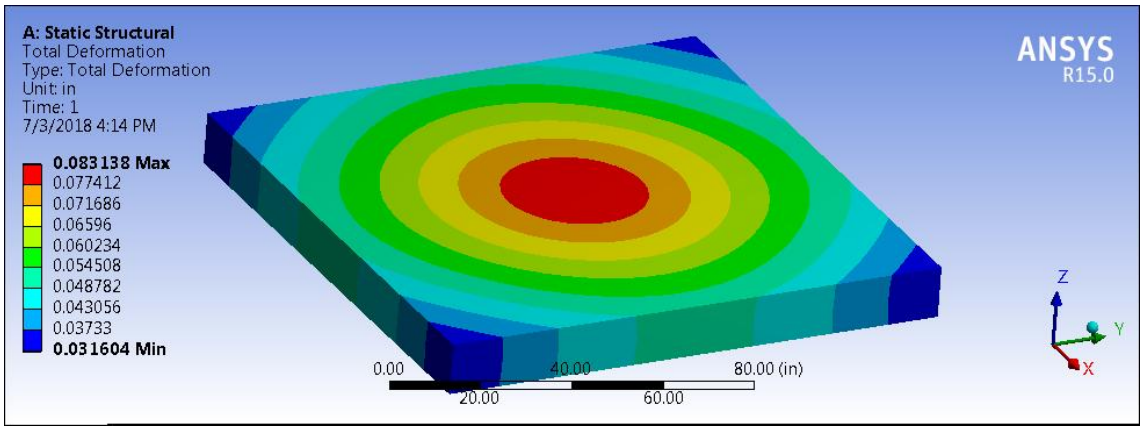

Figure (4.6) deflection occurred in the pavement and maximum deflection is under the load patch.

Table (4.2) shows the results of stresses and deflection of 3D model obtained the maximum and minimum values.

Table 4.4 maximum and minimum stresses and deflection results using finite element

Method	Stresses (psi)		Deflection (in)	
	Max	Min	Max	Min
ANSYS Program	1096.4	0.6654	0.083138	0.031604

4.3 Comparison Results:

From above results (stress and deflection) between the analytical method and finite element method, the maximum stress in finite element analysis occurs actually under the aircraft tire imprint is 41.4 % more than stress of analytical method occurs in any point in centerline actually causes about 30 (in) from the load position in finite element model are presents in figure 4.8 and the maximum deflection in finite element analysis occurs actually under the aircraft tire imprint is 22.4 % more than deflection of analytical method occurs in any point in centerline actually causes about 20 (in) from the load position in the finite element model are presents in figure 4.9.

Then, the numerical 3D modelling method using computer code ANSYS is concluded a reliable method for the determination of the stress and deflection in the concrete slab. The differences between this method and the 2D method are due to the difference in the adopted assumptions such as reference temperature compressive strength, coefficient of thermal expansion of concrete materials and the friction ratio between the layers (slab and foundation).

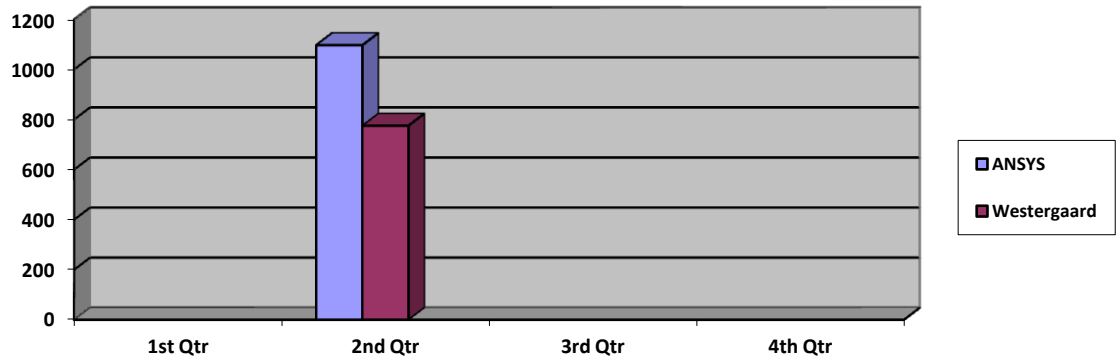

Figure (4.8): comparison between Westergaards and FE stresses results.

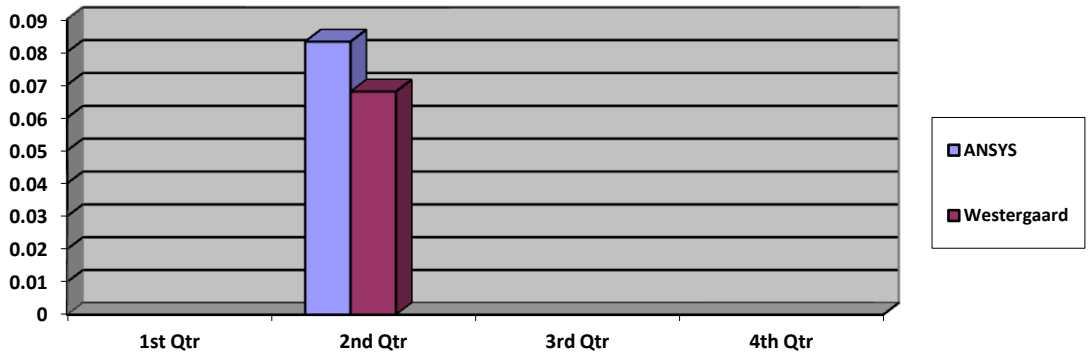

Figure (4.9): comparison between Westergaards and FE deflection results.

\

CHAPTER FIVE
CONCLUSION AND RECOMMENDATION

5.1 Conclusion

Investigation of behavior prediction of airport concrete pavement leads to the realization that the behavior of airport pavement is highly complex. The reaction of the pavement to design aircraft loading can be described by a large number of parameter each dependent on a set of variables. The fatigue cracks and erosion in concrete pavement causes by over stresses. this study illustrates the use of finite element method, in the analysis of rigid pavement systems subject to interior loading. It is shown that the finite element method is capable of simulating the observed responses of rigid pavement subject to pressure of design aircraft. The work described in this study deals with the finite element modelling for obtaining the maximum stresses and deflections in concrete slab and comparing with westergaards solutions. Results derived from analysis and comparison lead to the following secondary conclusions:

1. Position of maximum stresses and deflection are predominantly closer to the center of slab.

2. 3DFEA by using ANSYS are very close to Westergaard's closed form solution for interior loading condition by more than 70% nearest.

3. Finite Element Method can be applicable and reliable tool for analysis of runways concrete pavement.

3.2 Recommendations

As a result of this study it is recommended that the finite element program ANSYS is to be used for analysis, design, and sensitive studies of input parameters for concrete pavements.

For future studies the following is recommended:

1. Analysis of stress and deflection for the case when the aircraft load is applied at the edge and corner of the runway concrete slab and compare with the ANSYS model

2. Stress and deflection analysis for the multi layers (concrete pavement, base and subbase) should be further investigated for the case when a full circular dual and tandem load is applied at the interior, edge and corner of the pavement

3. Calculation stress and deflection in airport pavements, due to the variation of the material properties and dynamic load (Non Linear analysis)

4. Creation of a new model of ANSYS including the reinforcements concrete (ties and bars) and elastic joints and analysis of stress and deflection with static and dynamic load of aircraft for single slab and multilayer's and determined of maximum tensile stress comparing with analytical method

5. Creation of new model of stress and deflection of flexible airport pavement with different asphalt materials properties and dynamic load

6. Verification of the stress-based pavement model by comparing the prediction of deflection and stress from the aircraft stress by using 2D methods and compare with the 3D model.

REFERENCES

1. Brill,D. (2011) , Review of 10 years of concrete pavement studies at yhe NAPTF,FAA, 2nd international conference on best practice for concrete pavements, Brasil

2. Cirak, F.,Dere,Y., Sotelino,E. and Archer,G.(2016), Finite Element Formulation for Plates, Handout 3 , Cambridge University, UK.

3. Chen, H. etal,(2002), Mid-Panel cracking of Portland cement concrete pavement in India, Final report, FHWA.

4. Huang, Y. H., (2004), Pavement Analysis and Design. New Jersey: Pearson Prentice Hall

5. Melaku, S., and Hongsheng, (2015), Q., "Finite Element Analysis of Pavement Design Using ANSYS Finite Element Code." The Second International Conference on Civil Engineering, Energy and Environment, pp. 64-69

6. Patil S. S1and Khurd.V. G2, (2016), A Study of Static Response of Concrete Pavement Resting on Elastic Foundation, International Journal of Innovative Research in Science, Engineering and Technology.

7. Rehman M.T etal,(2011), Stress-Strain characteristics of flexible pavement using funite element Analysis, International Journal of civil and structural engineering , Volume 2, No 1

8. Wei Tu, M.S, 2007, Response Modelling of Pavement Subjected to Dynamic Surface Loading Based on Stress-Based Multi-Layered Plate Theory, Ohio State University.

9. Westergaard, H. M., (1976), Stresses in concrete pavements computed by theoretical analysis, Public Roads, Vol. 7, No. 2, pp. 25-35,1926.

10. Yoder, E. J., and Witczak, M. W., (1976), Principles of Pavement Design, Second Edition

11. Zdiri,M., (2009), Modelling of the Stresses and Strains Distribution in an RCC Pavement Using the Computer Code "Abaqus", Electronic Journal of Structural Engineering

Appendix (A) : ANSYS Report

Project

First Saved	Friday, June 29, 2018
Last Saved	Tuesday, July 03, 2018
Product Version	15.0 Release
Save Project Before Solution	No
Save Project After Solution	No

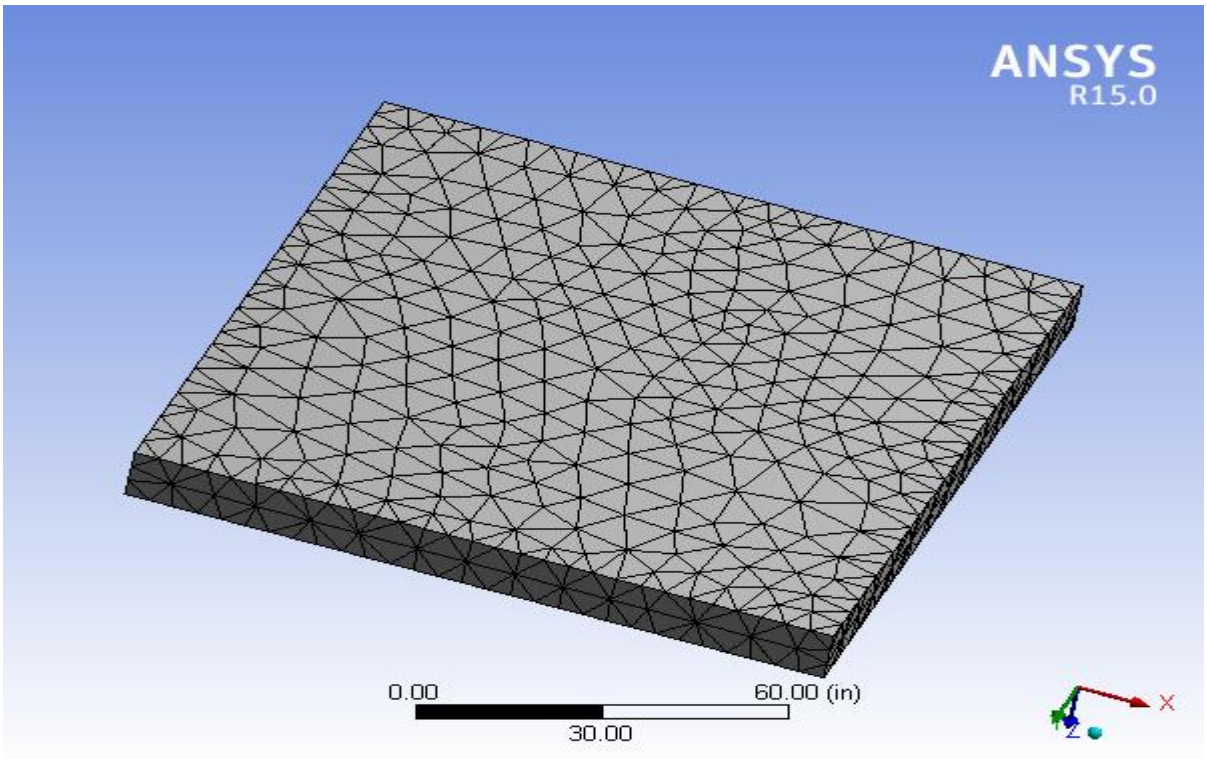

Contents

- **Units**
- **Model (A4)**
  - Geometry
    - Solid
  - Coordinate Systems
  - Connections
    - Contacts
  - Mesh
  - Mesh Numbering
  - **Static Structural (A5)**
    - Analysis Settings
    - Loads
    - Solution (A6)
      - Solution Information
      - Results
- **Material Data**
  - Concrete

Units

TABLE A-1

Unit System	U.S. Customary (in, lbm, lbf, s, V, A) Degrees rad/s Fahrenheit
Angle	Degrees
Rotational Velocity	rad/s
Temperature	Fahrenheit

Model (A4)

Geometry

TABLE A-2
Model (A4) > Geometry

Object Name	*Geometry*
State	Fully Defined
Definition	
Source	C:\Users\DELL\Desktop\New folder (2)\pavement\md3_files\dp0\SYS\DM\SYS.agdb
Type	DesignModeler
Length Unit	inches
Element Control	Program Controlled
Display Style	Body Color
Bounding Box	
Length X	120. in
Length Y	120. in
Length Z	12. in
Properties	
Volume	1.728e+005 in³
Mass	14358 lbm

Scale Factor Value	1.
Statistics	
Bodies	1
Active Bodies	1
Nodes	5529
Elements	2904
Mesh Metric	None
Basic Geometry Options	
Parameters	Yes
Parameter Key	DS
Attributes	No
Named Selections	No
Material Properties	No
Advanced Geometry Options	
Use Associativity	Yes
Coordinate Systems	No
Reader Mode Saves Updated File	No
Use Instances	Yes
Smart CAD Update	No
Compare Parts On Update	No
Attach File Via Temp File	Yes
Temporary Directory	C:\Users\DELL\AppData\Roaming\Ansys\v150
Analysis Type	3-D
Decompose Disjoint Geometry	Yes
Enclosure and Symmetry Processing	Yes

TABLE A-3
Model (A4) > Geometry > Parts

Object Name	*Solid*
State	Meshed
Graphics Properties	
Visible	Yes
Definition	
Suppressed	No
Stiffness Behavior	Flexible
Coordinate System	Default Coordinate System
Reference Temperature	By Environment
Material	
Assignment	Concrete
Nonlinear Effects	Yes
Thermal Strain Effects	Yes
Bounding Box	
Length X	120. in
Length Y	120. in
Length Z	12. in
Properties	
Volume	1.728e+005 in³
Mass	14358 lbm
Centroid X	60. in
Centroid Y	60. in

Centroid Z	-6. in
Moment of Inertia Ip1	1.7402e+007 lbm·in²
Moment of Inertia Ip2	1.7402e+007 lbm·in²
Moment of Inertia Ip3	3.446e+007 lbm·in²
Statistics	
Nodes	5529
Elements	2904
Mesh Metric	None

Coordinate Systems

TABLEA- 4
Model (A4) > Coordinate Systems > Coordinate System

Object Name	*Global Coordinate System*
State	Fully Defined
Definition	
Type	Cartesian
Coordinate System ID	0.
Origin	
Origin X	0. in
Origin Y	0. in
Origin Z	0. in
Directional Vectors	
X Axis Data	[1. 0. 0.]
Y Axis Data	[0. 1. 0.]
Z Axis Data	[0. 0. 1.]

Connections

TABLE A-5
Model (A4) > Connections

Object Name	*Connections*
State	Fully Defined
Auto Detection	
Generate Automatic Connection On Refresh	Yes
Transparency	
Enabled	Yes

TABLE A- 6
Model (A4) > Connections > Contacts

Object Name	*Contacts*
State	Fully Defined
Definition	
Connection Type	Contact
Scope	
Scoping Method	Geometry Selection
Geometry	All Bodies
Auto Detection	
Tolerance Type	Slider
Tolerance Slider	0.
Tolerance Value	0.42532 in
Use Range	No

Face/Face	Yes
Face/Edge	No
Edge/Edge	No
Priority	Include All
Group By	Bodies
Search Across	Bodies

Mesh

TABLE A- 7
Model (A4) > Mesh

Object Name	*Mesh*
State	Solved
Defaults	
Physics Preference	Mechanical
Relevance	0
Sizing	
Use Advanced Size Function	Off
Relevance Center	Medium
Element Size	Default
Initial Size Seed	Active Assembly
Smoothing	Medium
Transition	Fast
Span Angle Center	Coarse
Minimum Edge Length	12.0 in
Inflation	
Use Automatic Inflation	None
Inflation Option	Smooth Transition
Transition Ratio	0.272
Maximum Layers	5
Growth Rate	1.2
Inflation Algorithm	Pre
View Advanced Options	No
Patch Conforming Options	
Triangle Surface Mesher	Program Controlled
Patch Independent Options	
Topology Checking	Yes
Advanced	
Number of CPUs for Parallel Part Meshing	Program Controlled
Shape Checking	Standard Mechanical
Element Midside Nodes	Program Controlled
Straight Sided Elements	No
Number of Retries	Default (4)
Extra Retries For Assembly	Yes
Rigid Body Behavior	Dimensionally Reduced
Mesh Morphing	Disabled
Defeaturing	
Pinch Tolerance	Please Define
Generate Pinch on Refresh	No
Automatic Mesh Based Defeaturing	On
Defeaturing Tolerance	Default
Statistics	

Nodes	5529
Elements	2904
Mesh Metric	None

TABLE A-8
Model (A4) > Mesh Numbering

Object Name	*Mesh Numbering*
State	Not Solved
Definition	
Node Offset	Default
Element Offset	Default
Compress Node Numbers	Yes

Static Structural (A5)

TABLE A-9
Model (A4) > Analysis

Object Name	*Static Structural (A5)*
State	Not Solved
Definition	
Physics Type	Structural
Analysis Type	Static Structural
Solver Target	Mechanical APDL
Options	
Environment Temperature	71.6 °F
Generate Input Only	No

TABLE A-10
Model (A4) > Static Structural (A5) > Analysis Settings

Object Name	*Analysis Settings*
State	Fully Defined
Step Controls	
Number Of Steps	1.
Current Step Number	1.
Step End Time	1. s
Auto Time Stepping	Program Controlled
Solver Controls	
Solver Type	Program Controlled
Weak Springs	Program Controlled
Large Deflection	Off
Inertia Relief	Off
Restart Controls	
Generate Restart Points	Program Controlled
Retain Files After Full Solve	No
Nonlinear Controls	
Newton-Raphson Option	Program Controlled
Force Convergence	Program Controlled
Moment Convergence	Program Controlled
Displacement Convergence	Program Controlled
Rotation Convergence	Program Controlled
Line Search	Program Controlled
Stabilization	Off

Output Controls	
Stress	Yes
Strain	Yes
Nodal Forces	No
Contact Miscellaneous	No
General Miscellaneous	No
Store Results At	All Time Points
Analysis Data Management	
Solver Files Directory	C:\Users\DELL\Desktop\New folder (2)\pavement\md3_files\dp0\SYS\MECH\
Future Analysis	None
Scratch Solver Files Directory	
Save MAPDL db	No
Delete Unneeded Files	Yes
Nonlinear Solution	No
Solver Units	Active System
Solver Unit System	Bin

TABLE A-11
Model (A4) > Static Structural (A5) > Loads

Object Name	*Pressure*	*Elastic Support*
State	Fully Defined	
Scope		
Scoping Method	Geometry Selection	
Geometry	1 Face	
Definition		
Type	Pressure	Elastic Support
Define By	Components	
Coordinate System	Global Coordinate System	
X Component	0. psi (ramped)	
Y Component	0. psi (ramped)	
Z Component	-292. psi (ramped)	
Suppressed	No	
Foundation Stiffness		200. lbf/in³

FIGURE A-1
Model (A4) > Static Structural (A5) > Pressure

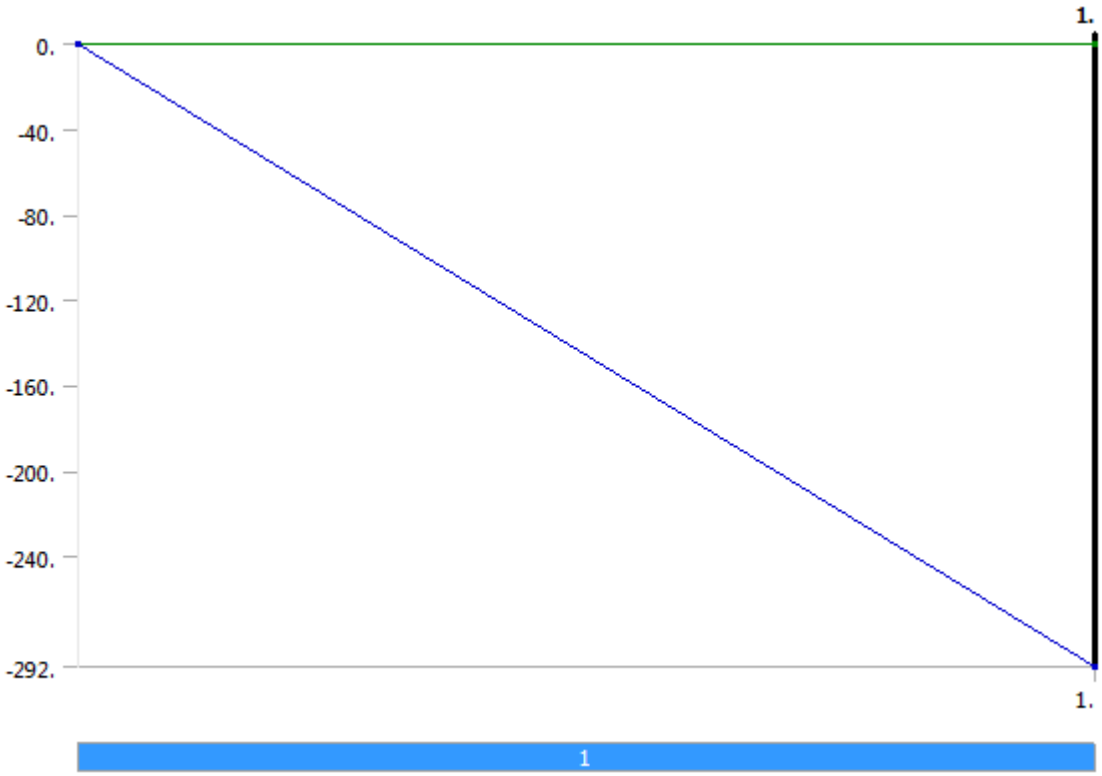

Solution (A6)

TABLE A-12
Model (A4) > Static Structural (A5) > Solution

Object Name	*Solution (A6)*
State	Obsolete
Adaptive Mesh Refinement	
Max Refinement Loops	1.
Refinement Depth	2.
Information	
Status	Solve Required

TABLEA- 13
Model (A4) > Static Structural (A5) > Solution (A6) > Solution Information

Object Name	*Solution Information*
State	Obsolete
Solution Information	
Solution Output	Solver Output
Newton-Raphson Residuals	0
Update Interval	2.5 s
Display Points	All
FE Connection Visibility	
Activate Visibility	Yes
Display	All FE Connectors
Draw Connections Attached To	All Nodes
Line Color	Connection Type
Visible on Results	No
Line Thickness	Single
Display Type	Lines

TABLE A- 14
Model (A4) > Static Structural (A5) > Solution (A6) > Results

Object Name	*Total Deformation*	*Equivalent Elastic Strain*	*Equivalent Stress*	*Maximum Shear Stress*	*Directional Deformation*
State	Obsolete				
Scope					
Scoping Method	Geometry Selection				
Geometry	All Bodies				
Definition					
Type	Total Deformation	Equivalent Elastic Strain	Equivalent (von-Mises) Stress	Maximum Shear Stress	Directional Deformation
By	Time				
Display Time	Last				
Calculate Time History	Yes				
Identifier					
Suppressed	No				
Orientation					X Axis
Coordinate System					Global Coordinate System
Results					
Minimum	3.1604e-002 in	1.6635e-007 in/in	0.6654 psi	0.37133 psi	-3.7966e-003 in
Maximum	8.3138e-002 in	2.745e-004 in/in	1096.4 psi	549.45 psi	3.7929e-003 in
Minimum Value Over Time					
Minimum	3.1604e-002 in	1.6635e-007 in/in	0.6654 psi	0.37133 psi	-3.7966e-003 in
Maximum	3.1604e-002 in	1.6635e-007 in/in	0.6654 psi	0.37133 psi	-3.7966e-003 in
Maximum Value Over Time					
Minimum	8.3138e-002 in	2.745e-004 in/in	1096.4 psi	549.45 psi	3.7929e-003 in
Maximum	8.3138e-002 in	2.745e-004 in/in	1096.4 psi	549.45 psi	3.7929e-003 in
Information					
Time	1. s				
Load Step	1				
Substep	1				
Iteration Number	1				
Integration Point Results					
Display Option		Averaged			
Average Across Bodies		No			

Material Data

Concrete

TABLE A-15
Concrete > Constants

Density	8.3093e-002 lbm in^-3
Coefficient of Thermal Expansion	1.e+007 F^-1
Specific Heat	0.1863 BTU lbm^-1 F^-1
Thermal Conductivity	9.6298e-006 BTU s^-1 in^-1 F^-1

TABLE A-16
Concrete > Compressive Ultimate Strength

Compressive Ultimate Strength psi
4619

TABLE A-17
Concrete > Compressive Yield Strength

Compressive Yield Strength psi
0

TABLE A-18
Concrete > Tensile Yield Strength

Tensile Yield Strength psi
0

TABLE A-19
Concrete > Tensile Ultimate Strength

Tensile Ultimate Strength psi
0

TABLE A-20
Concrete > Isotropic Secant Coefficient of Thermal Expansion

Reference Temperature F
-436.67

TABLE A-21
Concrete > Isotropic Elasticity

Temperature F	Young's Modulus psi	Poisson's Ratio	Bulk Modulus psi	Shear Modulus psi
	4.e+006	0.15	1.9048e+006	1.7391e+006

Appendix (B) : FAA report

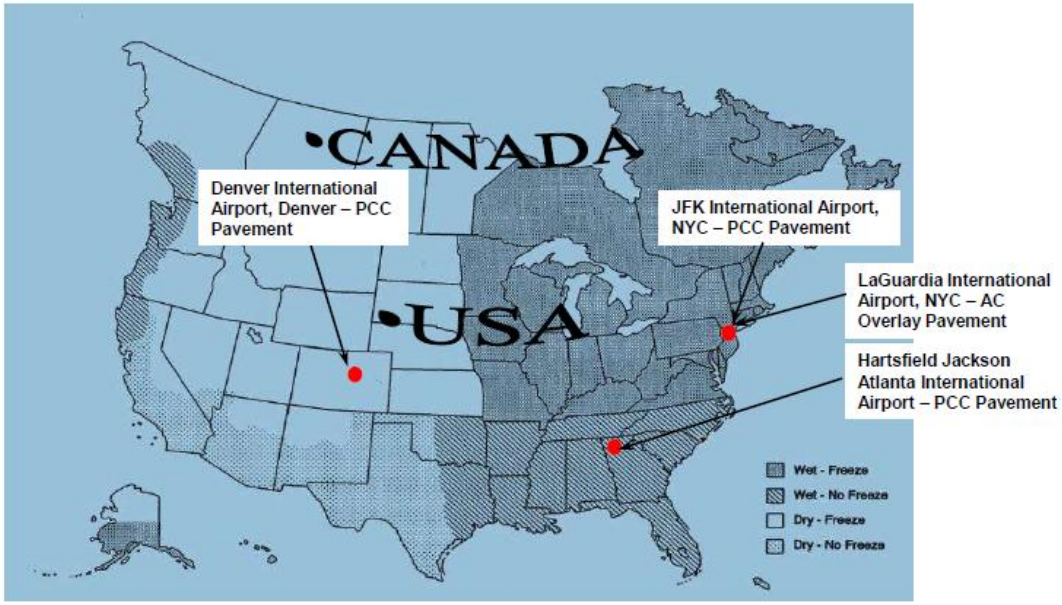

Figure (B-1) FAA Airport Instrumentation Projects

Figure (B-2) Single Slab Test

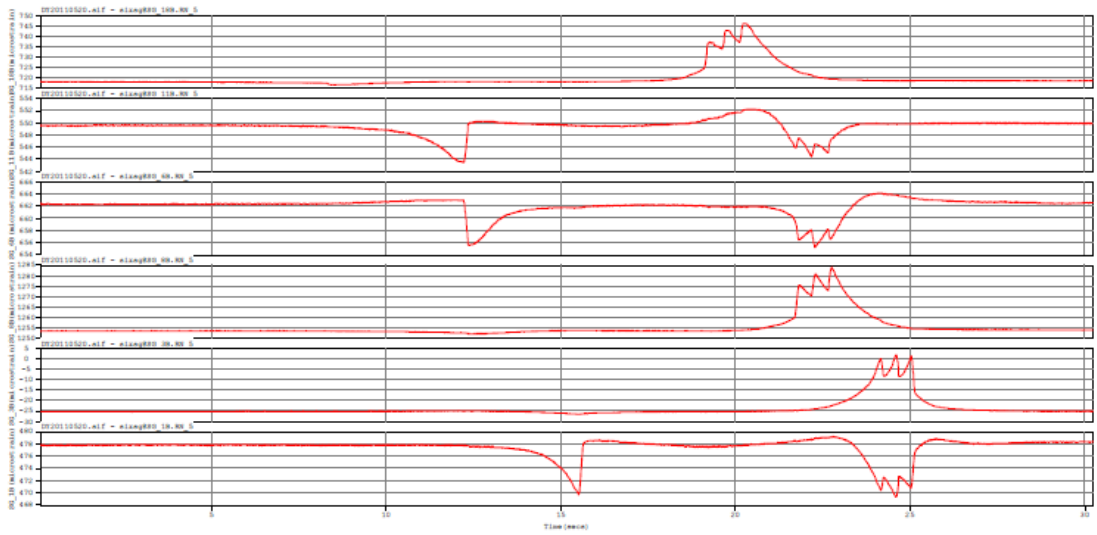

Figure (B-3) JFK – Typical Strain Responses

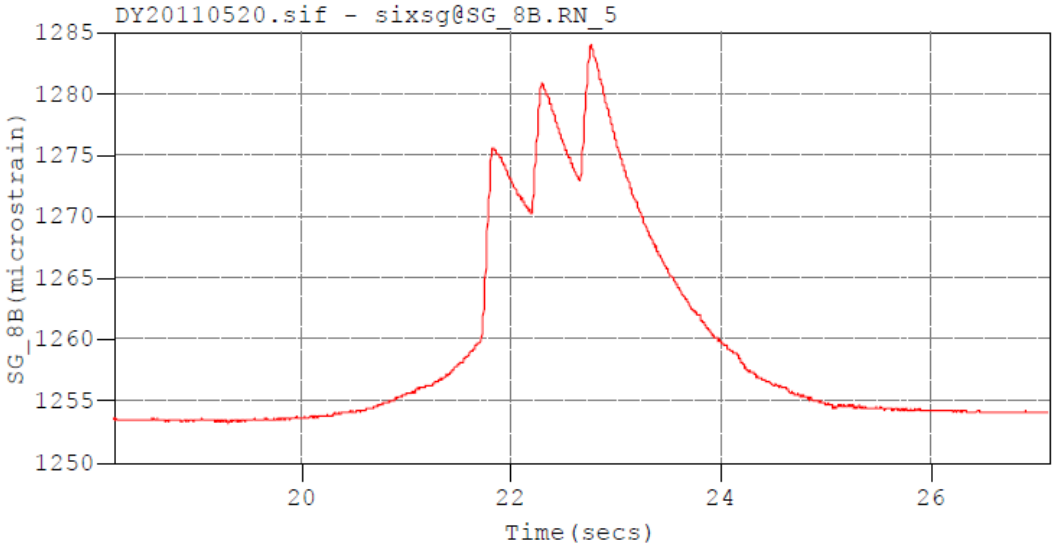

Figure (B-4) JFK – Detail – Gage 8B

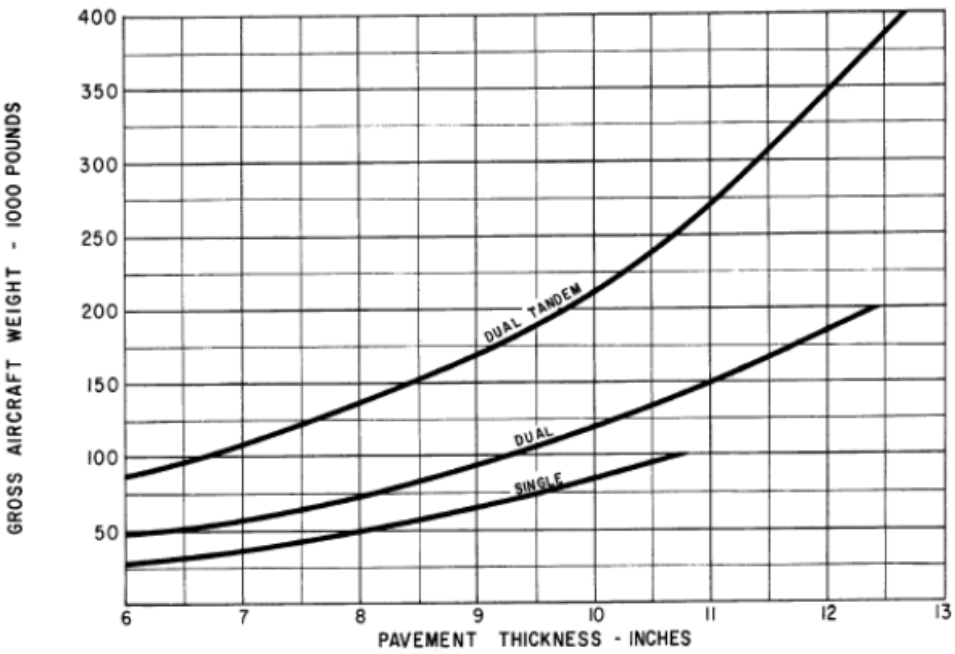

Figure (B-5) Critical stress was not directly involved in the thickness design.

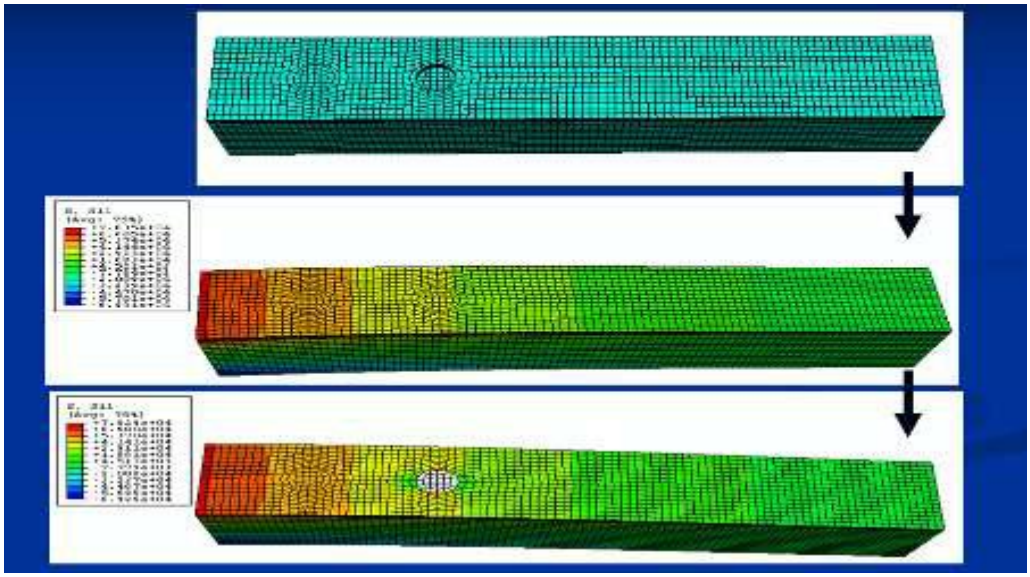

Figure (B-6) FAARFIELD model.

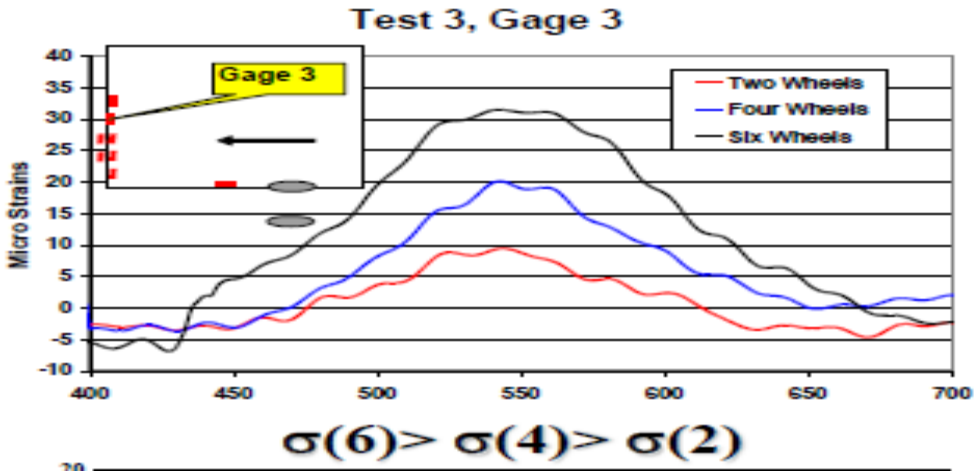

Figure (B-7) Surface Strain Gage Full-Scale Tests